ACSNANO

www.acsnano.org

ARTICLE

Artificial Cell Membrane Polymersome-Based Intranasal Beta Spike Formulation as a Second Generation Covid-19 Vaccine

Jian Hang Lam, Devendra Shivhare, Teck Wan Chia, Suet Li Chew, Gaurav Sinsinbar, Ting Yan Aw, Siamy Wong, Shrinivas Venkataraman, Francesca Wei Inng Lim, Pierre Vandepapeliere,* and Madhavan Nallani*

Cite This: *ACS Nano* 2022, 16, 16757−16775

Read Online

ACCESS | Metrics & More | Article Recommendations | Supporting Information

ABSTRACT: **Current parenteral coronavirus disease 2019 (Covid-19) vaccines inadequately protect against infection of the upper respiratory tract. Additionally, antibodies generated by wild type (WT) spike-based vaccines poorly neutralize severe acute respiratory syndrome coronavirus 2 (SARS-CoV-2) variants. To address the need for a second-generation vaccine, we have initiated a preclinical program to produce and evaluate a potential candidate. Our vaccine consists of recombinant Beta spike protein coadministered with synthetic CpG adjuvant. Both components are encapsulated within artificial cell membrane (ACM) polymersomes, synthetic nanovesicles efficiently internalized by antigen presenting cells, including dendritic cells, enabling targeted delivery of cargo for enhanced immune responses. ACM vaccine is immunogenic in C57BL/6 mice and Golden Syrian hamsters, evoking high serum IgG and neutralizing responses. Compared to an ACM-WT spike vaccine that generates predominantly WT-neutralizing antibodies, the ACM-Beta spike vaccine induces antibodies that neutralize WT and Beta viruses equally. Intramuscular (IM)-immunized hamsters are strongly protected from weight loss and other clinical symptoms after the Beta challenge but show delayed viral clearance in the upper airway. With intranasal (IN) immunization, however, neutralizing antibodies are generated in the upper airway concomitant with rapid and potent reduction of viral load. Moreover, antibodies are cross-neutralizing and show good activity against Omicron. Safety is evaluated in New Zealand white rabbits in a repeated dose toxicological study under Good Laboratory Practice (GLP) conditions. Three doses, IM or IN, at two-week intervals do not induce an adverse effect or systemic toxicity. Cumulatively, these results support the application for a Phase 1 clinical trial of ACM-polymersome-based Covid-19 vaccine (ClinicalTrials.gov identifier: NCT05385991).**

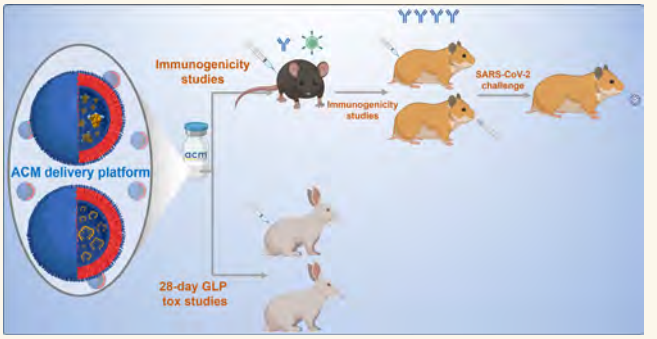

KEYWORDS: *ACM, polymersome, Covid-19, Beta spike, vaccine, intranasal*

Severe acute respiratory syndrome coronavirus 2 (SARS-CoV-2), the etiological agent of coronavirus disease 2019 (Covid-19), has spread rapidly worldwide since its discovery in December 2019 and continues to drive a global public health emergency. The situation is exacerbated by rapid viral evolution and the emergence of multiple SARS-CoV-2 variants, among which five variants of concern (VOCs) have been identified (https://www.who.int/en/activities/tracking-SARS-CoV-2-variants/): Alpha (B.1.1.7), first detected in the United Kingdom in September 2020; Beta (B.1.351) in South Africa, May 2020; Gamma (P.1) in Brazil, November 2020; Delta (B.1.617.2) in India, October 2020; Omicron (B.1.1.529) in Southern Africa, November 2021. VOCs are characterized by one or more of the following: increased transmissibility,[1,2] increased virulence,[3] or reduced effectiveness of public health and social measures or available diagnostics, vaccines, and therapeutics.[4−6] These features typically arise from the mutation of key residues within the spike protein. For instance, residue E484 within the receptor

Received: June 27, 2022
Accepted: October 6, 2022
Published: October 12, 2022

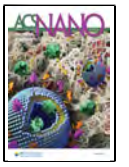

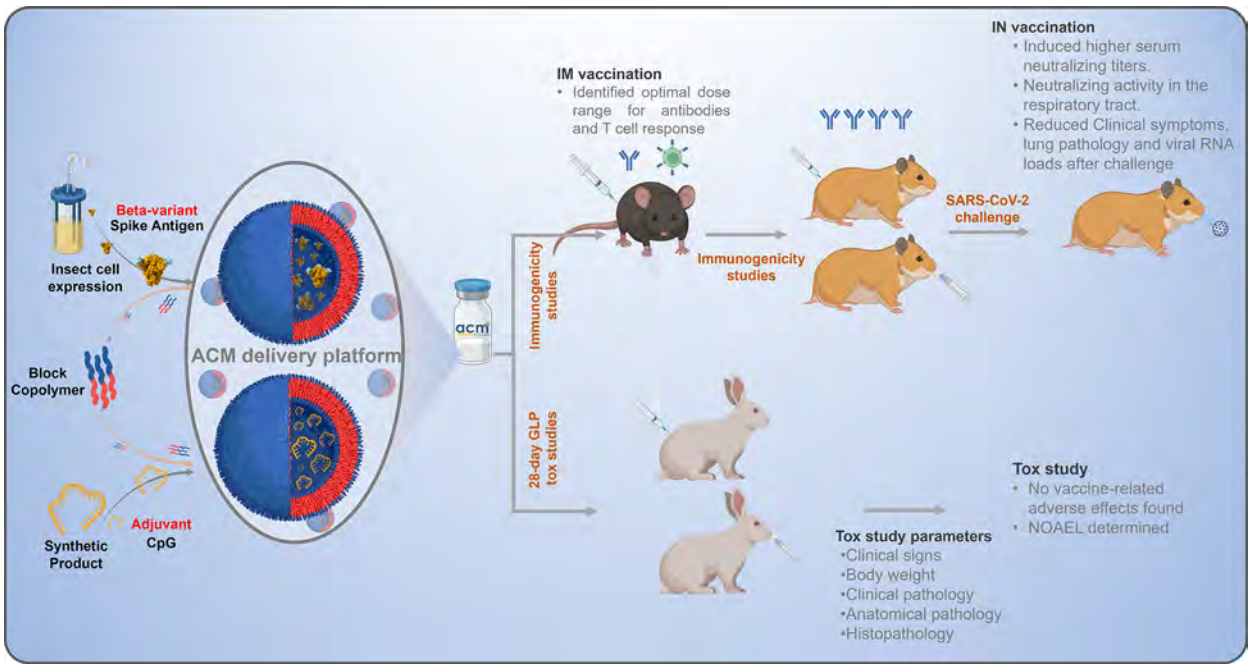

Figure 1. ACM-Covid-19 vaccine preclinical development program. The vaccine consisted of insect cell-produced recombinant spike protein and synthetic CpG adjuvant separately encapsulated in ACM polymersomes for coadministration. Immunogenicity was assessed in mice and hamsters after IM or IN administration. Protection against a live virus challenge was examined in hamsters. Key efficacy readouts are indicated. Safety was evaluated in a repeated dose GLP toxicological study in rabbits. Vaccine-related adverse effects were not detected.

binding domain (RBD) constitutes a dominant neutralizing epitope and is a site of principal importance.[7] The Omicron variant, in particular, has acquired more than 30 mutations (including the substitution mutation of E484) in the spike protein, which enable extensive neutralization escape from previously infected or vaccinated individuals.[5,8] Despite the reduction in neutralizing potency, primary vaccination with messenger ribonucleic acid (mRNA-1273; BNT162b2),[9] adenovirus vector (ChAdOx-1 S; Ad26.COV2.S),[10] and inactivated (CoronaVac; BBIBP-CorV)[11] formulations based on the wild type (WT) virus remains instrumental for the prevention of severe disease and death after infection by VOCs, possibly due to preservation of T cell reactivity toward conserved epitopes among variant spike proteins.[12−14] Moreover, boosting with mRNA vaccines has been shown to robustly enhance antibody titers and restore neutralizing activity toward Omicron.[5] However, breakthrough infections can still occur and are likely explained by a variety of factors, including failure to respond to vaccination due to young or old age or immunosuppressive disease, waning vaccine immunity, and failure to generate virus-specific IgA at the respiratory mucosa.[15]

It is desirable for a vaccine to induce broadly neutralizing responses toward all VOCs. Prior to the emergence of Omicron, the Beta variant consistently exhibited the strongest potential to evade neutralizing antibodies by the existing vaccines.[4,16,17] Interestingly, individuals who are infected by the Beta variant subsequently develop a vigorous antibody response that cross-neutralizes Alpha, Gamma, and Delta variants.[6,18−20] Approximately 40 human studies investigating the safety and efficacy of a Beta spike or RBD vaccine boost have been registered with ClinicalTrials.gov, indicating a keen interest in this approach. Here, we describe a strategy that combines the Beta antigen, polymersome delivery, and intranasal (IN) administration to elicit neutralizing antibodies systemically and in the respiratory tract. Recombinant Beta spike protein and synthetic CpG adjuvant are separately encapsulated within artificial cell membrane (ACM) polymersomes for coadministration. These synthetic nanovesicles measure 100−200 nm in diameter and are made up of an amphiphilic block copolymer comprising poly(butadiene)-*b*-poly(ethylene glycol) (PBD-*b*-PEO) and a cationic lipid, 1,2-dioleoyl-3-trimethylammonium-propane (DOTAP). We have previously shown ACM polymersomes to be efficiently taken up by antigen-presenting cells (APCs), including dendritic cells (DCs), thus enabling targeted delivery of encapsulated antigens and adjuvants for enhanced immune responses.[21] We and others have shown that the adjuvant effect of CpG is not impaired despite the lack of physical linkage to the antigen.[21,22] In this regard, our approach of codelivering spike protein and CpG in separate ACM vesicles confers flexibility in the choice of antigen to incorporate into the formulation, which is highly relevant given the rapid emergence of new VOCs.

In preparation for Phase 1 regulatory submission, we have established a preclinical program to produce ACM vaccines in-house and assess their safety and efficacy in different animal models. We first demonstrate that an ACM vaccine based on the Beta or WT spike is highly immunogenic in C57BL/6 mice and Golden Syrian hamsters after intramuscular (IM) administration. The WT spike vaccine generates antibodies that predominantly neutralize WT virus, whereas the Beta spike vaccine induces antibodies that cross-neutralize WT virus and the Beta variant. Subsequently, hamsters are challenged with live SARS-CoV-2 Beta variant to assess the protective efficacy of vaccination. Both vaccines strongly protect against weight loss and other clinical symptoms associated with the Beta challenge but show delayed viral clearance in the upper respiratory tract. Encouraged by the balanced neutralizing profile of the Beta spike vaccine, we further investigate IN

https://doi.org/10.1021/acsnano.2c06350
ACS Nano 2022, 16, 16757−16775

administration for its potential to enhance immunogenicity and protective efficacy.[23] IN administration of ACM-Beta spike vaccine induces neutralizing antibodies in the upper airway, which correlates with rapid and potent viral clearance after the challenge. Moreover, antibodies are broadly neutralizing and retain good activity against Omicron. To assess safety, a comprehensive 28-day Good Laboratory Practice (GLP) toxicological study is conducted in New Zealand white rabbits. The ACM-Beta spike vaccine exhibits an excellent safety profile after IM or IN administration with no adverse local effect or systemic toxicity being detected. Altogether, our preclinical program has successfully produced an ACM-Beta spike vaccine that satisfies safety and efficacy criteria for Phase 1 regulatory approval. Details of our ongoing clinical trial can be found at ClinicalTrials.gov (identifier: NCT05385991).

RESULTS AND DISCUSSION

Preclinical Program for the Production and Assessment of ACM-Covid-19 Vaccines. Figure 1 describes the key aspects of our preclinical ACM-Beta spike vaccine program. The process began with in-house expression and purification of recombinant spike protein followed by its encapsulation within ACM polymersomes. Synthetic CpG adjuvant was separately encapsulated. The final vaccine formulation consisted of both ACM-spike and ACM-CpG, as was previously described.[21] Immunogenicity of the ACM-Covid-19 vaccine was first determined in mice following IM injection, which represents a widely utilized route of administration in humans. Through dose escalation of antigen and adjuvant, we identified the effective dose range for an optimal antibody response. Subsequently, protective efficacy of the vaccine was tested in Golden Syrian hamsters against a live SARS-CoV-2 Beta variant challenge. Immunization was performed primarily by IM administration, but an IN vaccinated group was also included. Key readouts included serum IgG and neutralizing titers after immunization, and clinical symptoms, lung pathology, and viral RNA loads after the viral challenge. With the establishment of favorable immunogenicity and efficacy outcomes, we eventually proceeded with a comprehensive toxicological study in New Zealand white rabbits to identify potential safety signals after IM or IN administration.

To produce recombinant SARS-CoV-2 spike protein, Sf9 insect cells were transfected with recombinant baculovirus containing the gene encoding the spike ectodomain (hereby referred to as "S1S2") of SARS-CoV-2 Beta variant (B.1.351). The gene was strategically modified to encode two consecutive proline substitutions in the S2 subunit in a turn between the central helix and heptad repeat 1 (HR1) to stabilize the prefusion conformation.[24] This was considered desirable to generate relevant neutralizing antibodies.[25] In addition, three glutamine substitutions at the furin cleavage site were introduced to prevent separation of S1 and S2 subunits by cellular proteases. The secreted protein was purified from cell culture supernatant by sequential cation and anion exchange chromatography (Figure S1a,b, respectively). SDS-PAGE analysis of fractions collected over the purification process showed increasing purity of two closely migrating major bands at 150 kDa (Figure S1c). Further analysis by Western blot using a spike-specific polyclonal antibody (Figure S1e) and our previous experience with purifying WT spike[21] enabled us to ascertain their identity as the protein-of-interest (S1S2). Fractions with the highest purity from the Q column were pooled, and subsequent SDS-PAGE analysis confirmed the presence of major bands at 150 kDa as well as minor indistinct bands at 100 and 75 kDa (Figure S1d). Scanning densitometry consistently indicated a purity of >90%. Using a similar method, recombinant S1S2 protein from WT virus was also expressed and purified (Figure S1e).

To generate the vaccine formulation, S1S2(WT), S1S2-(Beta), and CpG 7909 adjuvant were separately encapsulated in ACM polymersomes, as was previously described.[21] Unlike the earlier mouse study, which utilized CpG 1826, a murine toll-like receptor 9 (TLR9) agonist, CpG 7909 was optimized for the stimulation of human TLR9,[26] had been evaluated in many clinical studies to be a safe and efficacious vaccine adjuvant,[27] and hence was incorporated in our human vaccine formulation for the present pivotal safety and efficacy assessment. Dynamic light scattering (DLS) measurements of ACM-S1S2(WT), ACM-S1S2(Beta), ACM-CpG, and the final vaccine formulation containing ACM-S1S2(WT) or ACM-S1S2(Beta) mixed with ACM-CpG revealed unimodal size distributions with average diameters of 169.4, 174.0, 135.8, 145.0, and 146.9 nm, respectively (Figure S1f), and polydispersity indices (PDI) that were consistently <0.17. Endotoxin content was quantified using the Endosafe cartridge from Charles River Laboratories, and the vaccine was released for animal experiments only if the endotoxin level was <10 EU/mL, based on a published recommendation for preclinical vaccine research.[28] Correspondingly, our preparations were consistently <5 EU/mL. To quantify the amount of encapsulated protein, polymersomes were lysed using 2.5−5% Triton X-100 and the lysate was analyzed using SDS-PAGE against a series of purified protein standards (Figure S1g). Encapsulated protein content, as determined by densitometric measurements, was 249.3 μg/mL (58% encapsulation efficiency) for S1S2(WT) and 389.1 μg/mL (56% encapsulation efficiency) for S1S2(Beta). ACM-CpG was similarly lysed and measured by reversed phase high performance liquid chromatography (RP-HPLC). Encapsulated CpG was determined to be 1047.6 μg/mL (75% encapsulation efficiency). The final vaccine formulation contained 15% w/w of spike antigen and 85% w/w of CpG. The function of S1S2 was evaluated through its ability to bind recombinant human angiotensin converting enzyme-2 (ACE2) in an enzyme-linked immunosorbent assay (ELISA). S1S2 was released from ACM polymersomes by Triton X-100 lysis, and detergent was largely removed using polystyrene adsorbent beads to reduce assay interference. S1S2(WT) and S1S2(Beta) in their respective final vaccine formulations were functional and bound plate-immobilized ACE2 with representative EC_{50} values of 78.0 and 58.8 ng/mL, respectively (Figure S1h).

ACM-WT Spike and ACM-Beta Spike Vaccines Induced Distinct Neutralization Profiles in Golden Syrian Hamsters. We had previously demonstrated that ACM-S1S2(WT) + ACM-CpG was highly immunogenic in mice and evoked strong and durable neutralizing titers.[21] In the present study, we continued our preclinical evaluation of two formulations containing ACM-Beta or ACM-WT S1S2 antigen with ACM-CpG adjuvant. A dose−response study was first performed in C57BL/6 mice to identify the optimal dose range of antigen and adjuvant, which would inform subsequent dose selection for hamster and human studies. Doses of antigen and adjuvant were selected on the basis of reported values in our earlier work[21] and elsewhere in the literature.[29−32] Mice were IM injected on Days 0 and 21

https://doi.org/10.1021/acsnano.2c06350
ACS Nano 2022, 16, 16757−16775

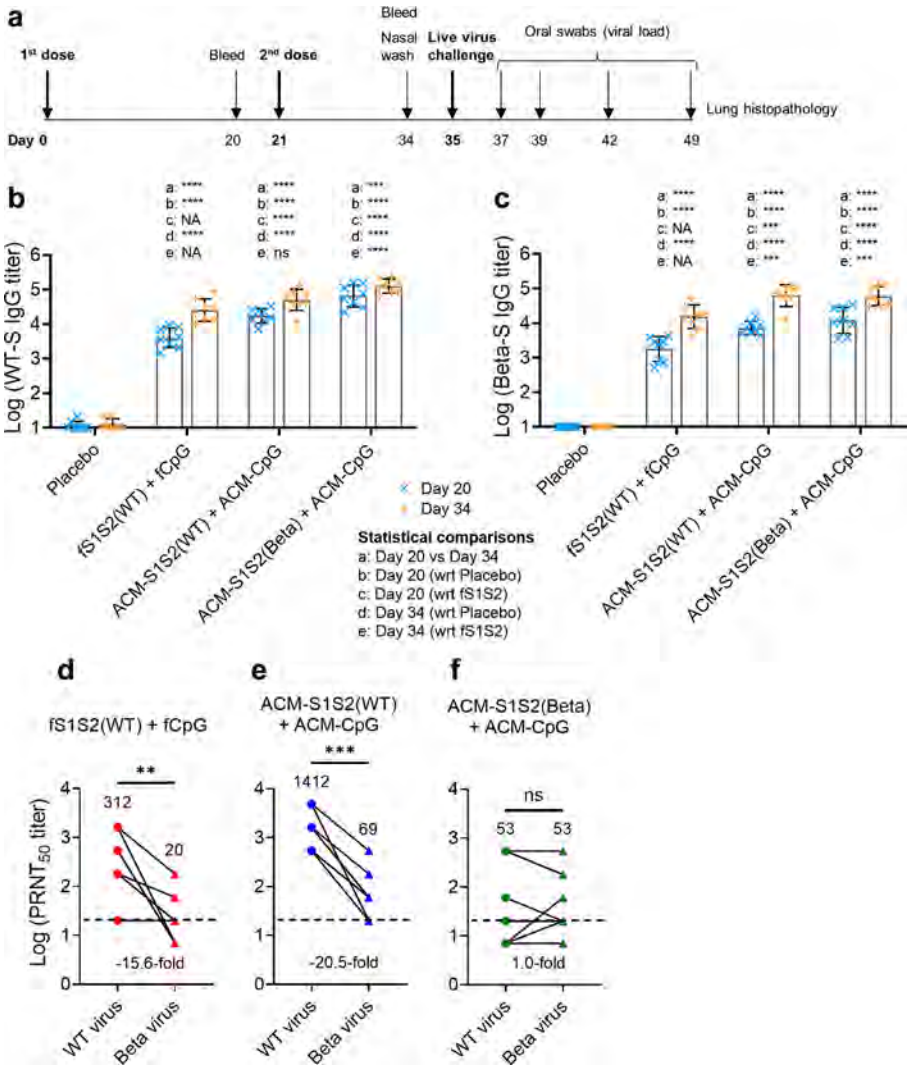

Figure 2. Serum antibody response to ACM-Covid-19 vaccines. (a) Immunization, sample collection, and live virus challenge schedule. Golden Syrian hamsters (n = 8) were IM administered one of the following: (i) PBS; (ii) fS1S2(WT) + fCpG; (iii) ACM-S1S2(WT) + ACM-CpG; (iv) ACM-S1S2(Beta) + ACM-CpG. (b, c) WT and Beta spike-specific serum IgG titers, respectively. The bar graph represents mean ± SD. Two-way repeated measures ANOVA with Tukey's or Šídák's multiple comparisons was performed. Significant differences between Day 20 and Day 34 IgG titers, between placebo and vaccinated animals, and between free S1S2(WT)-vaccinated and ACM-vaccinated animals are indicated for each time point. *: $P \leq 0.05$; **: $P \leq 0.01$; ***: $P \leq 0.001$; ****: $P \leq 0.0001$; ns: not significant; NA: not applicable. (d−f) Neutralizing potency toward WT virus or Beta variant. Geometric mean titers (GMTs) are indicated at the top of each graph; fold-change in GMT with respect to WT virus is indicated at the bottom. Lower limit of detection (1:20 serum dilution) is indicated by the horizontal dashed line. A two-tailed paired t test was performed.

(Figure S2a) with 0.12, 0.6, 3, or 15 μg of ACM-S1S2(Beta) together with 4, 20, or 100 μg of ACM-CpG at each dose level of antigen (doses hereby refer to the encapsulated spike protein or CpG adjuvant). Low-to-moderate serum IgG titers were generated after one dose and vigorously boosted by the second dose (Figure S2b−i). Antibodies strongly reacted with WT (Figure S2b,e) and Beta (Figure S2f−i) spikes, consistent with the high degree of identity (99%) between the two proteins. IgG titer increased from 0.12 to 3 μg of ACM-S1S2(Beta) (Figure S2b−d,f−h) before plateauing at 15 μg of antigen (Figure S2e,i). At this antigen level, similar IgG titers were generated with coadministration of 4, 20, or 100 μg of ACM-CpG. Assessment of the IgG1:IgG2c ratio revealed a predominance of IgG2c (Figure S2j), suggesting a Th1 biased immune response.[33] Assessment of anti-ACM IgG across all dose combinations of ACM-S1S2(Beta) + ACM-CpG showed an overall lack of response (Figure S2k), suggesting that ACM polymersomes did not readily evoke an antivector IgG response.

On the basis of these results, we selected 20 μg of ACM-S1S2 and 100 μg of ACM-CpG for the assessment of protective efficacy in a hamster model of SARS-CoV-2 infection. This also represented the highest human dose in our ongoing Phase 1 trial (ClinicalTrials.gov identifier: NCT05385991), which was designed to evaluate the ACM-Beta spike vaccine in a single ascending dose to identify the amount of spike antigen and CpG 7909 adjuvant needed for optimum safety and immunogenicity. Golden Syrian hamsters were IM injected two doses of vaccine, containing ACM-Beta or ACM-WT S1S2 protein with ACM-CpG 7909, on Days 0 and 21 (Figure 2a). Similar to the dose−response study in mice, spike-specific IgG was detected in hamsters after a single dose of any formulation and antibody titer was significantly boosted by the second dose (Figure 2b,c). Antibodies also

https://doi.org/10.1021/acsnano.2c06350
ACS Nano 2022, 16, 16757−16775

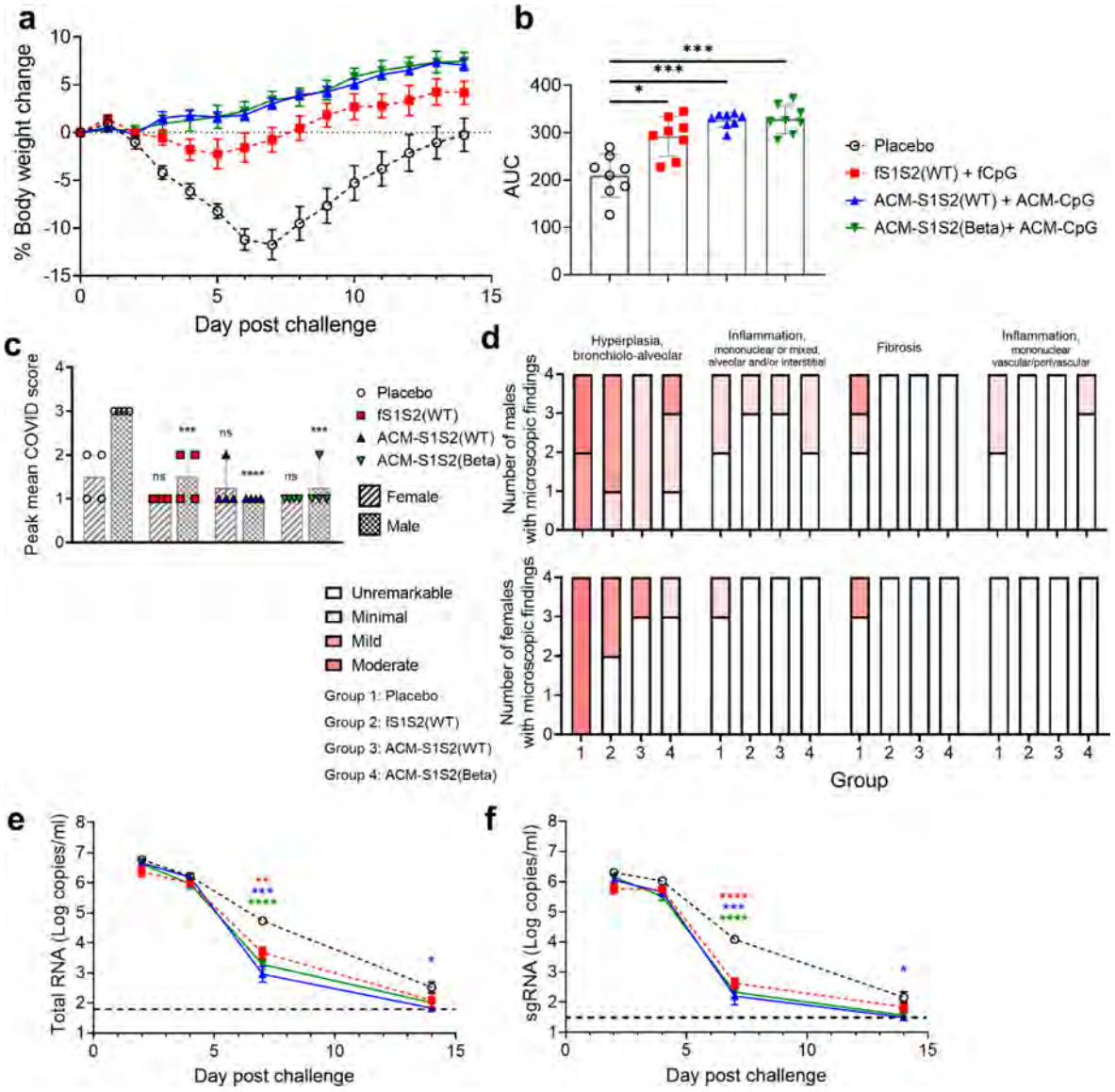

Figure 3. Live SARS-CoV-2 Beta variant challenge. Hamsters (n = 8) were inoculated with Beta variant via the intranasal route. (a) Changes in body weight over 14 days relative to the initial weight (horizontal dashed line). Mean ± SEM is shown. (b) Area under the curve (AUC) analysis for changes in body weight. Bar graph represents mean ± SD. Brown-Forsythe and Welch ANOVA with Dunnett's T3 multiple comparisons was performed. Only significant differences are shown. *: $P \leq 0.05$; **: $P \leq 0.01$; ***: $P \leq 0.001$. (c) Peak COVID scores of hamsters within 14 days after the virus challenge. Hamsters were observed daily for signs of disease (mild ruffled or ruffled fur, hunched back, labored/heavy breathing, and lethargy) or were noted as normal. Individual COVID scores were assigned (0 normal; ≤2 mild disease; 3 moderate disease; ≥4 severe disease). Plotted are individual peak COVID scores with average scores per group, gender depicted as bar graphs, and range depicted as whiskers. One-way ANOVA with Tukey's multiple comparisons was performed. Statistical significance with respect to gender-matched placebo controls is indicated above the bar graph. ***: $P \leq 0.001$; ****: $P \leq 0.001$; ns: not significant. (d) Histopathological analysis of SARS-CoV-2-related microscopic findings in lungs Day 14 post-challenge. Lungs of male (top) and female (bottom) hamsters were collected, fixed, processed to H&E-stained sections, and evaluated by a board-certified pathologist. Microscopic findings (hyperplasia, inflammation, and fibrosis) were scored according to severity and size of involved tissue or noted as unremarkable. (e, f) Viral RNA loads in oral swabs as determined by qPCR. Copy numbers (mean ± SEM) of total and subgenomic RNA (sgRNA) are shown, respectively. Horizontal dashed lines represent lower limits of detection (62 and 31 RNA copies/mL, respectively). Two-way repeated measures ANOVA with Tukey's multiple comparisons was performed. Only significant differences with respect to placebo controls are shown. *: $P \leq 0.05$; **: $P \leq 0.01$; ***: $P \leq 0.001$; ****: $P \leq 0.0001$.

reacted strongly with both WT and Beta spikes. Compared to the nonencapsulated WT spike formulation (i.e., fS1S2 + fCpG), the ACM-S1S2(WT) + ACM-CpG vaccine induced significantly higher IgG after one or two doses, indicating enhancement of immunogenicity through ACM encapsulation. Geometric mean titers (GMTs) of 5.1×10^4 against the WT spike and 6.3×10^4 against the Beta spike were elicited by the ACM-WT spike vaccine. A similar or higher titer was observed after immunizing with the ACM-Beta spike vaccine, which generated a GMT of 1.3×10^5 against the WT spike and 6.0×10^4 against the Beta spike.

Serum neutralizing activity was assessed using a plaque reduction neutralization test (PRNT) against SARS-CoV-2 WT or Beta virus. Antibodies elicited by IM administration of

https://doi.org/10.1021/acsnano.2c06350
ACS Nano 2022, 16, 16757−16775

fS1S2(WT) + fCpG or ACM-S1S2(WT) + ACM-CpG neutralized the WT virus 15−20-fold more efficiently than the Beta virus (Figure 2d,e), though neutralization of Beta still largely exceeded baseline (GMT ≥ 20). Notably, the ACM-S1S2(WT) + ACM-CpG vaccine induced approximately 3-fold higher neutralizing titer than the fS1S2(WT) + fCpG formulation, consistent with the enhancement of immunogenicity by ACM encapsulation. It was previously reported that infection by the Beta variant induced antibodies that efficiently cross-neutralized ancestral virus.[19,20] Consistent with that finding, hamsters vaccinated IM with the ACM-Beta spike vaccine generated antibodies that neutralized WT and Beta viruses equally, though the response was modest with a GMT of 53 (Figure 2F).

Real world data had established that antibodies generated by Covid-19 vaccines based on the WT virus exhibited a loss of neutralizing potency toward SARS-CoV-2 VOCs to varying extents. The most severe reduction occurred with the heavily mutated Omicron variant, which resulted in 18−100% neutralization escape in human subjects across studies.[5,12,34] Encouraged by the balanced $PRNT_{50}$ titers elicited by the ACM-Beta spike vaccine in hamsters, we asked whether such antibodies could cross-neutralize other VOCs. To answer this question, we examined the serum neutralizing activity of C57BL/6 vaccinated IM with an optimal dose of ACM-S1S2(Beta) + ACM-CpG from our earlier dose−response study (Figure S2l). Sera were evaluated with the FDA-approved, clinically validated surrogate virus neutralization kit (cPass),[35] which determined the neutralizing activity on the basis of the extent by which antibodies blocked the interaction between human ACE2 receptor and viral RBD. A balanced neutralization profile was observed against Alpha, Gamma, and Delta variants with an average inhibition of 70−84%. Importantly, neutralizing activity persisted against the Omicron (BA.1) variant with an average inhibition of 63.5%. The ability of ACM-Beta spike vaccine to trigger a T cell response was also examined. Splenic $CD44^{hi}$ memory phenotype $CD4^+$ T cells responded to *ex vivo* stimulation with an overlapping spike peptide pool by vigorous IFNγ and slight IL-5 production (Figure S2m−q), indicating a Th1-biased response. Antigen-specific $CD8^+$ T cell activity was also detected, which was dominated by IFNγ followed by some IL-2 production (Figure S2r−t). Altogether, these results suggested that the ACM-Beta spike vaccine could induce cross-neutralizing antibodies effective against multiple VOCs, including Omicron. Moreover, a Th1-biased, spike-specific T cell response was generated.

Our hamster experiments demonstrated that the WT spike vaccine induced robust homologous neutralizing titers that were markedly less efficacious toward the Beta variant, whereas the Beta spike vaccine elicited modest but balanced neutralizing titers. Nevertheless, the total IgG titer induced by either spike protein was comparable and reacted strongly against WT and Beta antigens. These observations suggested that B cell epitopes presented by WT and Beta spike to the immune system were largely similar but pronounced differences existed in terms of neutralizing epitopes. Accordingly, epitope mapping using human convalescent plasma showed the class 2 neutralizing epitope centered on position 484 to be immunodominant for ancestral SARS-CoV-2, whereas the class 3 epitope spanning sites 443 to 452 was immunodominant for the Beta variant.[36] Interestingly, a macaque vaccination study that investigated WT RBD prime followed by Beta RBD boost demonstrated an increased breadth of neutralizing response toward multiple VOCs.[37] In the context of our ongoing Phase 1 trial, which would evaluate safety and efficacy of an ACM-Beta spike boost in subjects who received primary vaccination with the WT spike, we speculated that a potential benefit from the introduction of Beta spike epitopes was the broadening of the neutralizing antibody repertoire, which may better protect against future SARS-CoV-2 variants.

A limitation of the present study was the inability to investigate T cell responses in hamsters as commercial antibodies to assess hamster T cell subsets and functions were unavailable.[38] Nevertheless, our earlier[21] and current mouse studies established that functional $CD4^+$ and $CD8^+$ T cells were elicited by ACM vaccines. Unlike neutralizing antibodies, which generally exhibited narrow target specificity, T cells demonstrated a high degree of cross-reactivity that stemmed from highly conserved epitopes.[14] Accordingly, $CD4^+$ and $CD8^+$ T cells from a previous vaccination or infection retained robust activity against Omicron, despite the variant's extensive mutations and increased resistance to neutralizing antibodies.[12,13] Cross-reactive T cells may contribute to a reduction in disease severity after infection by VOCs[14] and, hence, constitute an important layer of protection.

IM Vaccination with ACM Vaccines Protected Hamsters from Disease but Not Infection of the Upper Airway Following a Live SARS-CoV-2 Beta Challenge. The protective efficacy of each ACM Covid-19 vaccine was assessed using a nonlethal model of Beta infection. Clinical symptoms (weight loss, ruffled fur, hunched back, labored/heavy breathing, and lethargy) were monitored over 14 days post-challenge. Nonvaccinated animals lost up to 13% of initial body weight by Day 7 post-challenge before recovering through Day 14 (Figure 3a). Animals IM immunized with fS1S2(WT) + fCpG became mildly symptomatic after the viral challenge, losing approximately 3% of initial weight through Day 5 before recovering, indicating partial protection. In contrast, hamsters IM immunized with ACM-S1S2(WT) or ACM-S1S2(Beta) vaccine exhibited progressive weight gain over the 14-day study period. Area under the curve (AUC) analysis revealed significantly higher body weight gain in hamsters immunized with the fS1S2 + fCpG or ACM-S1S2 + ACM-CpG formulation compared to the nonvaccinated controls (Figure 3b), confirming the ability to protect against infection-associated weight loss. No significant difference was found between ACM-encapsulated and nonencapsulated formulations. Female hamsters were previously shown to be less susceptible to SARS-CoV-2 infection and disease.[39] Accordingly, when placebo- or fS1S2(WT) + fCpG-treated hamsters were examined on the basis of gender (Figure S3a,c, respectively), females showed a trend of reduced weight loss or faster weight recovery compared to males, though AUC analyses did not reveal significant differences (Figure S3b,d). In terms of Beta neutralizing antibody titers, no significant differences were found between females and males IM immunized with fS1S2(WT) + fCpG, ACM-S1S2(WT) + ACM-CpG, or ACM-S1S2(Beta) + ACM-CpG (Figure S3e−g, respectively), indicating that the increased resistance of female hamsters to Beta virus was not due to higher levels of neutralizing antibodies. In terms of clinical appearance, nonvaccinated controls presented with mild ruffled fur or occasionally ruffled fur, alone or in combination with a hunched back, with some showing lethargy and listlessness.

https://doi.org/10.1021/acsnano.2c06350
ACS Nano 2022, 16, 16757−16775

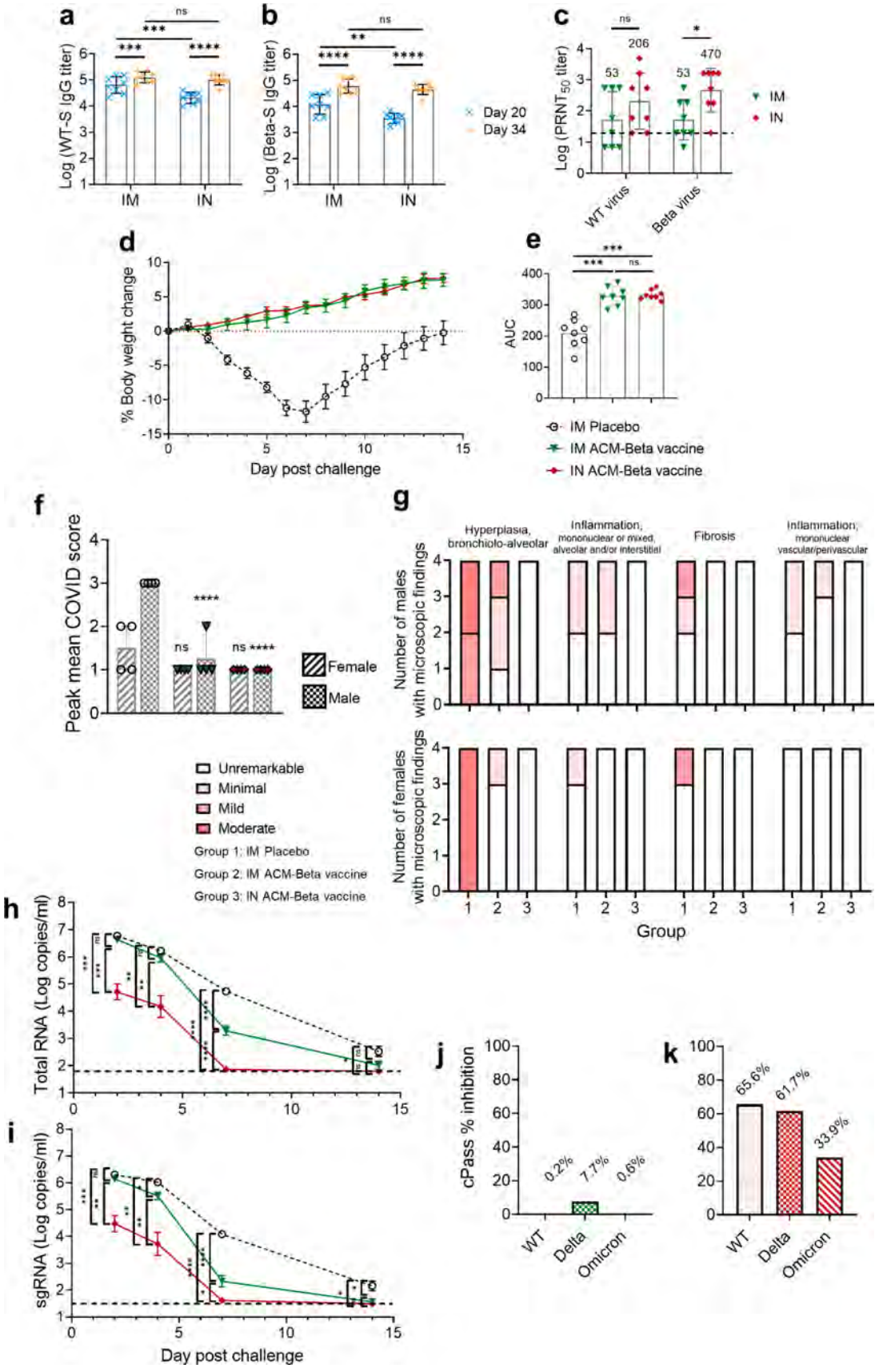

Figure 4. IN administration enhanced the immunogenicity of ACM-S1S2(Beta) + ACM-CpG and induced neutralizing antibodies in the upper airway. Hamsters (n = 8) were IM or IN administered an identical dose of ACM-S1S2(Beta) + ACM-CpG on Days 0 and 21. (a, b) WT and Beta spike-specific serum IgG titers, respectively. Bar graph represents mean ± SD. Two-way repeated measures ANOVA with Šidák's multiple comparisons was performed. *: $P \leq 0.05$; **: $P \leq 0.01$; ***: $P \leq 0.001$; ****: $P \leq 0.0001$; ns: not significant. (c) Neutralizing

https://doi.org/10.1021/acsnano.2c06350
ACS Nano 2022, 16, 16757−16775

Figure 4. continued

potency toward WT virus or Beta variant. Bar graph represents mean ± SD. Geometric mean titers (GMTs) are shown on top of the bar graphs. Lower limit of detection (1:20 serum dilution) is indicated by the horizontal dashed line. A two-tailed paired *t* test was performed. (d) Changes in body weight following the intranasal challenge with live SARS-CoV-2 Beta variant. Animals were monitored for 14 days. Initial body weight is indicated by the horizontal dashed line. Mean ± SEM is shown. (e) Area under the curve (AUC) analysis for changes in body weight. Bar graph represents mean ± SD. Brown-Forsythe and Welch ANOVA with Dunnett's T3 multiple comparisons was performed. (f) Peak mean COVID scores of hamsters within 14 days after the virus challenge. Hamsters were observed daily for signs of disease such as mild ruffled or ruffled fur, hunched back, labored/heavy breathing, and lethargy or were noted as normal. Individual COVID scores based on clinical observation were assigned (0 normal, ≤2 mild disease, 3 moderate disease, ≥4 severe disease). Plotted are individual peak COVID scores (individual data points) and mean peak COVID scores per group and gender (bar) with the range (whiskers). One-way ANOVA with Tukey's multiple comparisons was performed. A significant difference with respect to gender-matched placebo controls is indicated, where present. (g) Histopathological analysis of SARS-CoV-2-related microscopic findings in hamster lungs Day 14 post-challenge. Lungs of male (top) and female (bottom) hamsters were collected, fixed, processed to H&E-stained sections, and evaluated by a board-certified pathologist. Microscopic findings (hyperplasia, inflammation, and fibrosis) were scored according to the severity and size of the involved tissue. (h, i) Viral RNA loads in oral swabs as determined by qPCR. Copy numbers (mean ± SEM) of total and subgenomic RNA (sgRNA) are shown, respectively. Horizontal dashed lines represent lower limits of detection (62 and 31 RNA copies/mL, respectively). Two-way repeated measures ANOVA with Tukey's multiple comparisons was performed. *: $P \leq 0.05$; **: $P \leq 0.01$; ***: $P \leq 0.001$; ****: $P \leq 0.0001$; ns: not significant. (j, k) Neutralizing activity of nasal washes from hamsters IM or IN immunized, respectively. Neutralization of RBD from WT, Delta, or Omicron virus was determined using a cPass kit (% inhibition indicated above the bar graphs). To overcome their highly dilute nature, nasal washes from each group were pooled and concentrated 40-fold.

Females generally presented with a low COVID score of 1 that transiently increased to 2, whereas males consistently presented with a score of 3 from Days 6 to 12 post-challenge (Figure 3c). Importantly, peak COVID scores for all immunized male hamsters were significantly lower than those for the corresponding placebo controls (Figure 3c), suggesting that immunization resulted in reduced disease severity.

Histopathological analysis of lung tissue was performed at the conclusion of the challenge period. Incidence and severity of bronchiolo-alveolar hyperplasia, alveolar and/or interstitial mononuclear or mixed inflammation, fibrosis, and vascular/perivascular mononuclear inflammation in the lung were assessed (see Figure S4a–d for representative images). SARS-CoV-2-related findings were decreased in all immunized groups compared to placebo-treated animals (Figure 3d). Moreover, females exhibited lower incidence and severity of lung pathology in all immunized groups compared to males, consistent with their higher resistance to SARS-CoV-2.[39]

To assess viral load after infection, oral swabs were collected 2, 4, 7, and 14 days after the challenge (Figure 2a) and subjected to viral RNA qPCR. Nonvaccinated controls exhibited a peak viral RNA load of 5.8×10^6 copies/mL (geometric mean) on Day 2, which gradually declined to 1.6×10^6 copies/mL on Day 4 and finally to 3.3×10^2 copies/mL on Day 14 (Figure 3e). Hamsters IM immunized with fS1S2(WT) + fCpG, ACM-S1S2(WT) + ACM-CpG, or ACM-S1S(Beta) + ACM-CpG did not differ in peak viral load from nonvaccinated controls on Days 2 to 4 but cleared the virus more efficiently by Day 7. Subgenomic RNA (sgRNA) analysis was performed to gain insight into viral replication.[40] In nonvaccinated controls, the kinetics of viral sgRNA were similar to total RNA with a peak viral load of 2.0×10^6 copies/mL on Day 2 followed by a decline to 1.1×10^6 copies/mL on Day 4 and finally 1.4×10^2 copies/mL on Day 14 (Figure 3f). Hamsters IM immunized with an ACM-encapsulated or nonencapsulated formulation showed similar sgRNA levels on Days 2 and 4 as the nonvaccinated controls, before a sharp decline on Day 7 and eventually approaching the lower limit of detection on Day 14. Cumulatively, the results indicated that ACM-WT or Beta spike vaccine strongly protected hamsters from infection-associated weight loss and substantially reduced the severity of clinical symptoms, particularly among males. Nevertheless, delayed viral clearance in the upper respiratory tract and residual SARS-CoV-2-associated lung pathology 14 days after the challenge represented major limitations of the current vaccination approach.

IN Administration of ACM-Beta Spike Vaccine Enhanced Its Immunogenicity and Protective Efficacy. The ACM-Beta spike vaccine showed good potential in its ability to evoke cross-neutralizing antibodies after IM administration, but delayed viral clearance and incomplete protection from lung pathology after the viral challenge remained an issue. Several studies had demonstrated that IN vaccination was associated with the induction of an adaptive immune response at the respiratory tract, increased immunogenicity, and reduced viral shedding after the SARS-CoV-2 challenge in various animal models, compared to the IM vaccination.[23,41] The impact of the route of administration on immunogenicity was evaluated by comparing the antibody response of hamsters IM or IN immunized with ACM-S1S2(Beta) + ACM-CpG. Serum IgG generated by IN vaccination reacted strongly with WT and Beta spike proteins (Figure 4a,b). IgG titer on Day 20 was significantly lower than that by IM administration but was boosted by the second dose to a comparable level as IM vaccination on Day 34. Strikingly, serum $PRNT_{50}$ titers against WT and Beta viruses were increased 4- and 9-fold, respectively, after IN vaccination (Figure 4c). Vaccinated hamsters were subsequently challenged with SARS-CoV-2 Beta variant and monitored over 14 days for body weight changes and other clinical symptoms. IN vaccination strongly protected animals from infection-associated weight loss (Figure 4d), and AUC analysis indicated significantly higher body weight gain compared to placebo controls and similar weight gain as IM-vaccinated hamsters (Figure 4e). Further evaluation of clinical symptoms showed IN-vaccinated hamsters to consistently present with a low peak COVID score of 1 in both males and females, unlike their IM-vaccinated counterparts, which occasionally presented with a score of 2 (Figure 4f). Moreover, histopathological examination of lungs at the conclusion of the study did not find evidence of infection-associated pathology in all IN-vaccinated animals (Figure 4g; see also Figure S4e for a representative H&E image). With regard to viral RNA loads in oral swabs collected across the challenge study, IN vaccination was

https://doi.org/10.1021/acsnano.2c06350
ACS Nano 2022, 16, 16757–16775

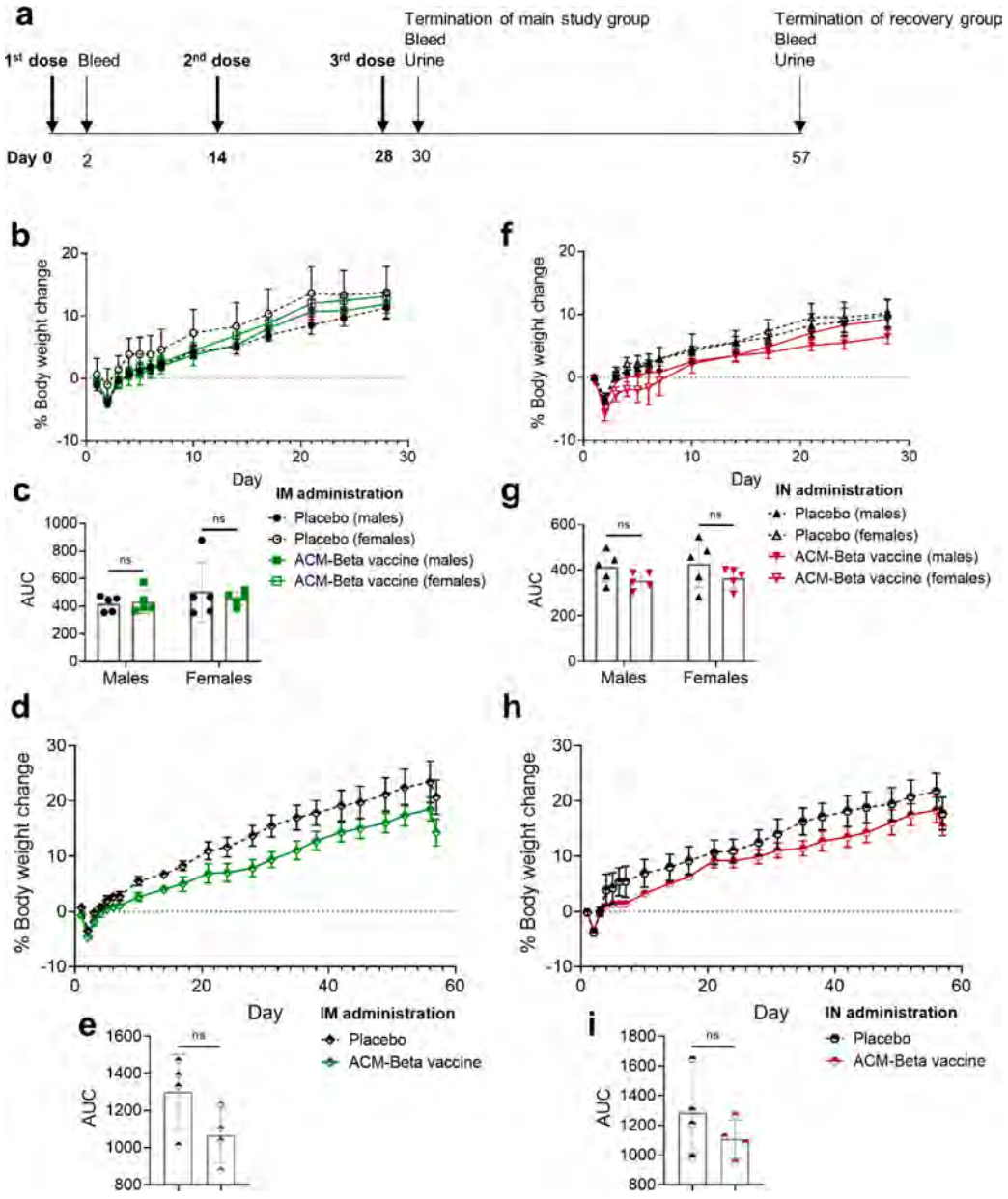

Figure 5. Body weight changes in rabbits IM or IN administered ACM-S1S2(Beta) + ACM-CpG. (a) Immunization and sample collection schedule. New Zealand white rabbits were administered 0.5 mL of 20 μg of ACM-S1S2(Beta) + 100 μg of ACM-CpG 7909 on Days 0, 14, and 28. IM injection was performed on the left quadriceps muscle on Days 0 and 28 and on the right on Day 14. IN was performed with 0.25 mL per nostril. Rabbits were segregated into a main study group (five males and five females) and a recovery group (two males and two females). (b, f) Changes in body weight of the main study group over 28 days after IM or IN administration, respectively. Male and females were analyzed separately. Initial body weight is indicated by the horizontal dashed line. Mean ± SEM is shown. (c, g) Area under the curve (AUC) analysis for changes in body weight after IM or IN administration, respectively. Bar graph represents mean ± SD. Two-way ANOVA with Sidák's multiple comparisons was performed. ns: not significant. (d, h) Changes in body weight of the recovery group over 57 days after IM or IN administration, respectively. Males and females were combined for analysis. (e, i) AUC analysis for changes in body weight after IM or IN administration, respectively.

associated with rapid and potent viral clearance, unlike IM vaccination (Figure 4h,i). Compared to nonvaccinated controls, the average viral RNA load of IN-vaccinated hamsters was ~100-fold lower on Days 2 and 4 (5.1×10^4 and 1.5×10^4 RNA copies/mL, respectively) and dropped to the lower limit of detection on Day 7 (Figure 4h). Likewise, sgRNA showed a 60−200-fold drop on Days 2 to 4 (3.0×10^4 and 5.3×10^3 copies/mL, respectively) and reached the lower limit of detection on Day 7 (Figure 4i).

To elucidate the mechanism of viral clearance, nasal washes collected on Day 34 were analyzed using the cPass kit for neutralizing activity. As the samples were highly dilute, they were pooled and concentrated 40-fold before analysis. Neutralizing activity against the RBD of WT, Delta, or Omicron (BA.1) virus was not detected in nasal washes from IM-immunized hamsters (Figure 4j), suggesting an absence of neutralizing antibodies that contributed to delayed viral clearance in the upper respiratory tract (Figure 3e,f). In contrast, nasal washes from IN-vaccinated hamsters showed

https://doi.org/10.1021/acsnano.2c06350
ACS Nano 2022, 16, 16757−16775

clear neutralizing activity against WT and Delta viruses with inhibitions of 65.6% and 61.7% being detected, respectively (Figure 4k). Even against the Omicron RBD, an inhibition of 33.9% was observed. Cumulatively, we showed that IN but not IM administration of ACM-Beta spike vaccine in hamsters generated neutralizing antibodies in the respiratory tract, which correlated with rapid viral clearance after the SARS-CoV-2 challenge. Moreover, these antibodies appeared to cross-neutralize multiple VOCs, including Omicron, which was consistent with the neutralization data of our earlier mouse experiment (Figure S2l).

The weak protection against the infection of the upper respiratory tract after IM vaccination stemmed largely from its limited ability to induce an adaptive immune response at the respiratory mucosa despite potent systemic immune responses.[42] With the aim of evoking systemic and local immune responses, we performed IN administration of the ACM-Beta spike vaccine and observed enhanced serum neutralizing titers, rapid reduction in the viral RNA load in the upper respiratory tract after the challenge, and virus neutralizing activity in nasal washes. Moreover, only IN vaccinated hamsters did not present with any SARS-CoV-2-associated lung pathology at the conclusion of the challenge study. We were unable to measure spike-specific IgA titers as secondary antibodies targeting hamster IgA were not commercially available. Nevertheless, protection induced by IN vaccination was likely mediated by IgA, since mucosal IgA represented the primary form of adaptive immune protection in the upper respiratory tract.[43] Moreover, studies have shown that IgA can neutralize respiratory viruses in humans and animal models, thus serving as a potential correlate of protection.[44,45]

With more than 30 mutations in its spike protein, Omicron was shown to escape neutralizing antibodies elicited by past infection or immunization. Primary vaccination with mRNA (BNT162b; mRNA-1273), adenovirus vector (ChAdOx-1 S; Ad26.COV2.S), or subunit protein (NVX-CoV2373) vaccines based on the WT spike generated antibodies that poorly neutralized Omicron, leading to complete neutralization escape in 18−100% of vaccinees, depending on the study and the time after immunization.[5,12,34] Nevertheless, neutralizing activity was restored by boosting with mRNA vaccine encoding WT or Omicron spike.[5,46,47] Here, we showed that primary vaccination with ACM-S1S2(Beta) + ACM-CpG generated broadly neutralizing antibodies that retained activity toward Omicron. Furthermore, we could evoke neutralizing activity in the upper respiratory tract through IN vaccination. Enhanced transmissibility of the Omicron variant was believed to be caused, in part, by its robust infection of cells in the upper respiratory tract when compared to the ancestral virus or other variants.[48,49] Therefore, the ability to trigger neutralizing antibodies in the respiratory tract through IN vaccination would be critical for the effective control of Omicron infection and may be more relevant than boosters administered via IM injection.

One limitation of the IN vaccination study is the lack of an animal group immunized with free spike + free CpG to evaluate the baseline immunogenicity of the nonencapsulated formulation. Nevertheless, several lines of evidence suggest that ACM encapsulation should continue to drive an enhanced immune response in the IN setting. Most respiratory viruses have an average size ranging between 20 and 200 nm, and nanocarriers with comparable sizes (ACM polymersomes having a size range of 100−200 nm) are thought to follow a similar uptake pathway to the nasopharynx-associated lymphoid tissue (NALT),[50] which represents a key inductive tissue for mucosal immunity.[51] Moreover, the ability of ACM polymersomes to facilitate uptake by APCs is expected to remain important in the IN context for the efficient induction of adaptive immunity. Experimentally, IN administration of antigen ± CpG adjuvant encapsulated within liposomes[52] or polymeric nanocarriers formulated with poly(L-lactic acid) (PLA),[53] poly(lactic-*co*-glycolic acid) (PLGA) and chitosan,[54] or a pH-responsive diblock copolymer[55] has been shown to significantly improve the mucosal IgA or T cell response. In a separate mucosal vaccination study, we have orally administered pigs with ACM-encapsulated spike protein from the porcine epidemic diarrhea virus (PEDV) and observed enhanced virus-specific fecal swab IgA, compared to the administration of free antigen alone (data not shown). Cumulatively, we believe the existing data supports a role for ACM polymersomes in mucosal vaccine delivery and the enhancement of an immune response following IN administration.

ACM-S1S2(Beta) + ACM-CpG Exhibited an Excellent Safety Profile in Rabbits after IM or IN Administration. A toxicological study was conducted in New Zealand white rabbits to evaluate the safety of ACM-Beta spike vaccine. The rabbit is frequently used for the toxicity assessment of vaccines as it represents a species large enough to receive the full human dose.[56] Placebo or vaccine (corresponding to 20 μg of spike antigen and 100 μg of CpG 7909 per dose) was administered in a 0.5 mL volume for three doses on Days 0, 14, and 28 (Figure 5a). IM injection took place in the left quadriceps muscle on Days 0 and 28 and in the right muscle on Day 14. IN administration was given as a 0.25 mL dose per nostril using a Mucosal Atomization Device (MAD). The main study group consisted of five males and five females and was monitored over 28 days, whereas the recovery group consisted of two males and two females and was monitored for an additional 28 days to assess reversibility or persistence of toxic effects, if any. The full data set from this toxicological investigation is beyond the scope of this report; only the most crucial and relevant findings are presented. Rabbits administered IM or IN with ACM-Beta spike vaccine did not present with morbidity, mortality, or abnormal clinical signs. Local reactions (erythema and edema) at the injection and nasal administration sites were not detected. Progressive weight gain was observed in rabbits of the main study group (Figure 5b) and recovery group (Figure 5d) after IM injection with the ACM-Beta spike vaccine. Compared to the respective placebo controls, AUC analysis did not reveal significant differences for males or females (Figure 5c,e). Similarly, rabbits IN administered with the ACM-Beta spike vaccine showed steady weight gain (Figure 5f,h) and AUC analysis also did not reveal significant differences compared to the placebo controls (Figure 5g,i).

Blood was examined for vaccine-related effects on hematology, coagulation time, and clinical chemistry (see Tables S1−S3 for detailed parameters). There was no effect on coagulation and clinical chemistry parameters in both genders after IM administration of ACM-Beta spike vaccine. Adverse hematological parameters were not observed, though male rabbits did present with increases in neutrophils, lymphocytes, and monocytes on Day 30 (Table S4). These changes correlated with a significant increase in serum C-reactive protein (CRP) compared to placebo controls (Figure 6a) as

https://doi.org/10.1021/acsnano.2c06350
ACS Nano 2022, 16, 16757−16775

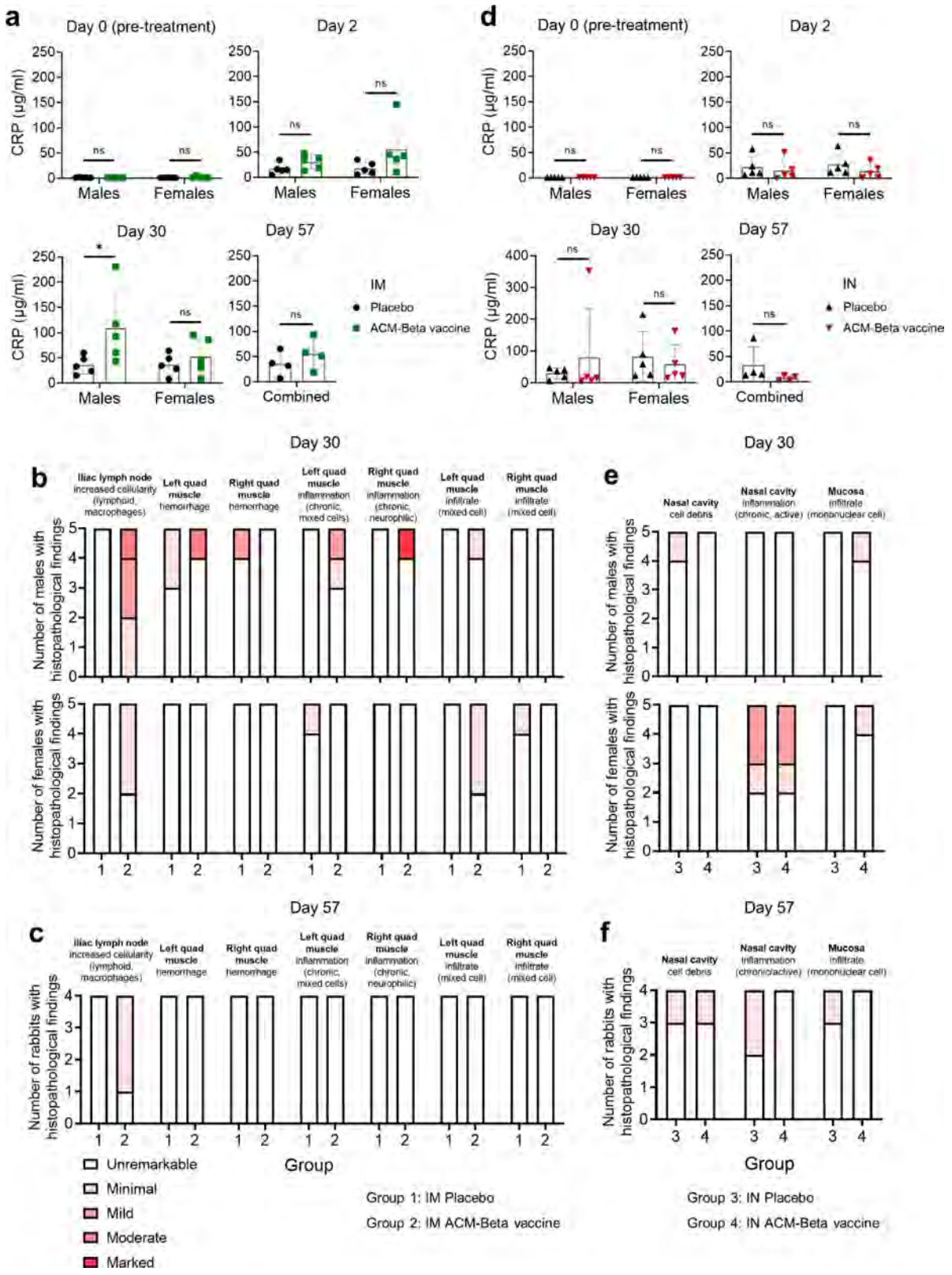

Figure 6. Serum C-reactive protein (CRP) levels and histopathological findings at the sites of administration. Rabbits were IM (a−c) or IN (d−f) administered placebo or ACM-S1S2(Beta) + ACM-CpG. (a, d) Serum CRP levels on Days 0, 2, 30, and 57. Data from Days 0, 2, and 30 was derived from the main study group (n = 10) and segregated on the basis of gender; data from Day 57 was derived from the recovery group (n = 4) and was not segregated. Two-way ANOVA with Šidák's multiple comparisons was performed. *: $P \leq 0.05$; ns: not significant. (b, c, e, f) Histopathological examination of the iliac lymph node, quadriceps muscle, and nose. Tissues were fixed, processed to H&E-stained sections, and evaluated by two pathologists. Microscopic findings (increased cellularity, hemorrhage, inflammatory infiltrate and cell debris) were scored according to severity. Analysis of the main study group on Day 30 (b, e) was segregated on the basis of gender, whereas the recovery group on Day 57 (c, f) was analyzed irrespective of gender.

https://doi.org/10.1021/acsnano.2c06350
ACS Nano 2022, 16, 16757−16775

well as the microscopic finding of mixed cell inflammation/infiltrates at the site of injection on Day 30 (Figure 6b). Hematological changes, elevated CRP (Figure 6a), and pathological changes at the site of injection (Figure 6c) were not detected at the end of the recovery period (Day 57). For rabbits IN administered with ACM-Beta spike vaccine, effects on hematology, coagulation, and clinical chemistry were not detected. Serum CRP levels between placebo and vaccinated animals were comparable at all time points, though one male presented with elevated CRP on Day 30 (Figure 6d). Urine collected at the termination of the main (Day 30) and recovery (Day 57) groups did not show vaccine-related effects (see Table S5 for detailed urinalysis parameters).

Anatomical and histopathological examination was performed at the termination of the main (Day 30) and recovery (Day 57) groups (see Table S6 for the list of organs examined). Major alterations in terminal body weights, organs weights and their ratios, and gross pathology were not detected after IM or IN vaccination. Microscopic findings at the injection site of IM groups (Figure 6b) generally included hemorrhages, chronic/mixed cell inflammation, or infiltrate of either macrophages or mixed cells in vaccinated and placebo control rabbits (see Figure S5 for representative images). The higher incidences and/or severity of chronic/mixed cell inflammation and mixed cell infiltrates noted in vaccinated animals when compared with the placebo control group were considered to be related to vaccine administration, which showed complete recovery on Day 57 (Figure 6c). The draining lymph nodes (iliac) showed increased macrophage/lymphoid cellularity on Day 30 (Figure 6b) characterized by the presence of predominantly increased lymphocytes in the cortex and medulla with the expansion of a germinal center with increased sinus macrophages in some animals. These changes were considered to be related to the vaccine and more frequently found in males than females. An increase in lymph node cellularity persisted until Day 57, albeit at a minimal level (Figure 6c).

IN administration did not induce a vaccine-specific adverse local or systemic effect in the main and recovery groups (Figure 6e,f). The few incidences of cell debris in the lumen (air passages and in the nasolacrimal duct/paranasal sinus) and chronic-active inflammation in the nasal cavity (see Figure S5 for the representative images) were distributed between vaccinated and placebo groups (Figure 6e) and thus not related to the vaccine formulation. The few incidences of all other microscopic findings observed in male and female rabbits were considered as incidental background findings and not related to vaccine administration as they were distributed randomly across the groups.

Cumulatively, a toxicological investigation established an excellent safety profile for the ACM-Beta spike vaccine following IM or IN administration. Rabbits did not present with adverse clinical signs, mortality, local reactions, and systemic toxicity. The only notable finding was increased cellular infiltrate and inflammation at the site injection (quadriceps muscle) along with increased cellularity of the muscle-draining iliac lymph node, both of which were an expected local response to vaccination. On the basis of these results, the "No Observed Adverse Effect Level" (NOAEL) of ACM-S1S2(Beta) + ACM-CpG 7909 in New Zealand white rabbits was considered three IM or IN administrations of 20 μg of antigen + 100 μg of adjuvant at two-week intervals.

CONCLUSIONS

The delivery of antigen and adjuvant to the immune system by nanocarriers can be achieved via surface attachment to or encapsulation within the carrier, each being associated with advantages and disadvantages that are well reported in the literature.[57,58] Conjugation of antigen to the surface of the nanocarrier facilitates a direct interaction with its cognate receptor but risks premature degradation by host enzymes. Encapsulation protects antigen and adjuvant from enzymatic degradation and facilitates controlled release, though the nanocarrier must first dissociate to release its cargo for receptor binding. We have chosen to encapsulate spike protein and CpG adjuvant within ACM polymersomes to leverage on the said advantages. Moreover, entrapping the antigen or adjuvant within polymersomes eliminates the need for additional surface functionalization,[59] which simplifies manufacturing. Importantly, we have shown previously[21] and in the current work that our formulation enhances the spike-specific antibody response, which indicates that encapsulation has not impaired the interaction with the cognate B cell receptor.

The currently described manufacturing processes of solvent dispersion, extrusion, and dialysis to produce vaccine formulations under Good Manufacturing Practice (GMP)-like conditions for preclinical safety and efficacy assessment have been scaled-up from an initial 5 mL to a liter scale batch size. To produce the drug product for a Phase 1 trial, these laboratory scale processes have been transferred to a GMP site and are replaced by continuous injection, homogenization, tangential flow filtration (TFF), and sterile filtration. These are commonly used unit operations in pharmaceutical manufacturing that still preserve the characteristics of the vaccine formulation.

The demonstration of ACM-vaccine safety with the IN route is significant for several reasons. A search through the ClinicalTrials.gov database shows all Covid-19 IN vaccine candidates to be viral-vectored formulations; no description of an mRNA vaccine delivered with lipid nanoparticles (LNPs) for clinical evaluation of IN administration can be found. We speculate one reason may be related to the report of excessive inflammation caused by the LNP carrier that results in the frequent death of animals.[60] With no precedence of a synthetic nanocarrier being clinically evaluated in the context of an IN Covid-19 vaccine, the approval of our polymersome-based IN vaccine for Phase 1 evaluation reflects the high degree of safety that is thoroughly demonstrated by our preclinical safety investigation.

METHODS

Production of Recombinant S1S2 Protein with an Sf9 Baculovirus System. The Beta variant spike protein ectodomain gene (amino acids 1−1201) containing the native signal peptide, 3Q mutations to the furin cleavage site, and 2P mutations was codon-optimized for insect cell protein expression using a GenScript proprietary algorithm and was directly synthesized into a pFASTBAC1 transfer plasmid. This transfer plasmid (500 ng) was transformed using heat shock (42 °C, 1 min) into competent DH10 BAC cells (Thermo Fisher Scientific). Cells were cultured on agar plates containing selection antibiotics and Blu-gal. Colonies that were positive for recombination were selected, and Bacmid DNA was extracted using traditional Midiprep technology. In brief, a 50 mL culture was inoculated from the plate and grown for 16 h at 37 °C and 200 rpm. The cells were pelleted, and the supernatant was removed. The pellet was resuspended into the resuspension buffer (25 mM Tris-HCl, pH 8, 10 mM EDTA, 100 μg/mL RNase) and allowed to

https://doi.org/10.1021/acsnano.2c06350
ACS Nano 2022, 16, 16757−16775

incubate at room temperature for 5 min, followed by incubation with lysis buffer (0.2 M NaOH and 1% SDS). Finally, precipitation buffer (3 M potassium acetate, pH 5.5) was added, and the solution was left to incubate for a further 10 min at 4 °C, followed by centrifugation at 10 000*g* and 4 °C for 15 min. The DNA was precipitated from the supernatant with 100% isopropanol and washed with 70% ethanol. The pellet was dried and finally resuspended in TE buffer, pH 8.0. This DNA was used for transfection using the methods described in the Bac-to-Bac (Thermo Fisher Scientific) with Trans IT-Virus GEN (Mirus). In brief, 2.4×10^5 Sf9 insect cells were plated into a well of a 24-well plate. After 1 h, the media was aspirated. A premix of transfection reagent and 200 ng of DNA was allowed to stand for 30 min at room temperature before being added to the plated cells. The plate was left to incubate for 6 h, followed by addition of the ESF-AF medium (Expression systems). Sf9 cells were left for 7 days at 27 °C without agitation. The baculovirus-containing supernatant was collected and used to infect further cultures of Sf9 cells to amplify various recombinant virus stocks (P1−P3). Finally, P3 virus stock was titrated as described[61] and used for protein expression.

Sf9 cells (Thermo Fisher Scientific) were routinely grown in ESF-AF medium and maintained at a cell density of $1-4 \times 10^6$ cells/mL. For protein production, cells were adjusted to $\sim 2 \times 10^6$ per mL in a 600 mL culture volume in a plastic 2 L nonbaffled flask. The culture was incubated to a density of $2.5-3 \times 10^6$ cells/mL and then infected with recombinant baculovirus (P3) at a multiplicity of infection (MOI) of 0.1. Flasks were left for 68−72 h at 27 °C with shaking at 115 rpm. To harvest spike protein secreted into the culture supernatant, cells were removed by centrifuging in a swing bucket rotor at 3000*g* and 4 °C for 10 min.

Protein Purification. A 50 kDa cutoff Tangential flow filtration column (Repligen) was washed and equilibrated as per the manufacturer's instructions. The harvested cell culture supernatant was then loaded onto the column, and the retentate was recirculated at a flow rate of 50 mL per minute. A 6−8 PSI transmembrane pressure was applied, and the sample was concentrated 10-fold and diafiltered 5 times with Buffer 1 (20 mM phosphate, 100 mM NaCl, 5% glycerol, pH 5). The final sample was centrifuged at 16 000*g* and 4 °C for 15 min. The supernatant was filtered through a 0.22 μm PES filter before subsequent purification steps.

A 1 × 5 mL GE Hitrap SP FF column and a 1 × 5 mL GE Hitrap Q HP column were used. Each column was pre-equilibrated using a GE AKTA FPLC Explorer with their respective binding buffer, i.e., 20 mM phosphate, 100 mM NaCl, 5% glycerol, pH 5 (Buffer 1) for the SP column and 20 mM phosphate, 100 mM NaCl, 5% glycerol, pH 8 (Buffer 2) for the Q column, with a flow rate of 2 mL/min for 10 column volumes (CV). The spike protein sample was placed on ice and loaded onto the SP column at 2 mL per minute until the entire sample was loaded. The unbound sample was collected for subsequent analysis. The column was washed with 10 CV of Buffer 1. After this, the bound protein on SP was eluted with Buffer 2 by switching the pH. The protein from this SP elution step was collected for further purification using the Q column. After 10 column volumes, the SP column was further eluted with Buffer 3 (20 mM phosphate, 1 M NaCl, 5% glycerol, pH 8), and the sample was collected for later analysis. Finally, the SP column was washed with 5 CV of 0.1 N NaOH, and the sample was collected for later analysis and stored. In the next step, the Buffer 2 eluate from the SP column was loaded onto the pre-equilibrated Q column until the entire sample was loaded. Following loading, the Q column was washed with Buffer 2 for another 10 column volumes. After the Q wash, a gradient between Buffer 2 and Buffer 3 was set from 0% to 32% for 75 min at 2 mL per minute. 5 mL fractions were collected across the linear gradients. The recombinant Beta variant spike (S1S2) protein eluted at a conductivity of 33−37 mS/cm (between 26% and 30% B).

Preparation of ACM-Antigen and ACM-CpG. Human CpG 7909 (T*C*G*T*C*G*T*T*T*T*G*T*C*G*T*T*T*T*G*T*-C*G*T*T, where * denotes a phosphorothioate bond) was synthesized by BioSpring. Murine CpG 1826 (T*C*C*A*-T*G*A*C*G*T*T*C*C*T*G*A*C*G*T*T) was purchased from InvivoGen. 1,2-Dioleoyl-3-trimethylammonium-propane (DOTAP) was from Avanti Polar Lipids. Triton X-100 was from MP Biomedicals. All other chemicals were purchased from Sigma-Aldrich unless stated otherwise. ACM polymersomes encapsulating the S1S2 protein were prepared by the solvent dispersion method, followed by extrusion. A 380 mg/mL stock solution of DOTAP and PEG_{13}-*b*-PBD_{22} polymer was prepared by dissolving solid DOTAP and polymer in tetrahydrofuran (THF) to prepare Solution A as described earlier.[21] A 5 mL solution of 600 μg/mL S1S2 protein was placed in a 50 mL Falcon tube (Solution B). Solution A was added slowly to 5 mL of Solution B while constantly mixing (600−700 rpm) at room temperature. A turbid solution was obtained. The resulting solution was extruded 21 times through a 200 nm membrane filter (Avanti Polar Lipids) using a 1 mL mini-extruder (Avanti Polar Lipids) to get monodispersed ACM-antigen vesicles. Nonencapsulated antigens were removed by 2 days of overnight dialysis with three buffer exchanges. The encapsulation of the antigen was quantified by densiometric analysis using known S1S2 protein standards in Fiji ImageJ software (v. 1.52a). ACM-CpG was prepared by the solvent dispersion method described above, followed by extrusion. 1.2 mL of the 700 mg/mL stock solution containing DOTAP and PEG_{13}-*b*-PBD_{22} polymer was added dropwise to a 10 mL CpG solution. A turbid solution was obtained. The resulting solution was extruded 21 times through a 200 nm membrane filter using a 1 mL mini-extruder to get monodispersed ACM-CpG polymersomes. Unencapsulated CpG was removed by overnight dialysis using a 300 kDa molecular weight cutoff (MWCO) as described earlier.[21] Dynamic light scattering (DLS) was performed on the Zetasizer Nano ZS system (Malvern Panalytical) to determine the sizes of vesicles. The endotoxin content of the ACM preparations was determined using the Endosafe cartridge from Charles River Laboratories.

ACE2-Binding Assay. ACM-S1S2 was lysed with 1% v/v Triton X-100 for 10 min at room temperature. Detergent was then removed by incubating with Bio-Beads SM-2 Resin (Bio Rad) with periodic agitation for 1 h at room temperature. Recombinant ACE2 protein (Sino Biological) in a high binding 96-well EIA/RIA plate (Corning) was coated in bicarbonate-carbonate buffer (pH 9.6) at 5 μg/mL overnight at 4 °C. The next morning, the plate was washed 4× with Tris-buffered saline + 0.05% v/v Tween-20 and blocked with 2% w/v bovine serum albumin (BSA). This and subsequent steps were performed at room temperature. S1S2 protein was 3-fold serially diluted to obtain a range of concentrations (0.61−12 000 ng/mL) and applied to plate-bound ACE2 for 2 h. The plate was washed 4×, and a murine monoclonal antibody recognizing the S1 domain (clone 1035206; R&D Systems) was applied at a 1:100 dilution for 2 h. The plate was washed 4× again, and HRP-conjugated goat antimouse IgG (H/L) was applied at 1:3000 (Bio Rad) for 1 h. Then, the plate was washed 4× and TMB substrate (Sigma-Aldrich) was added for 10 min, after which Stop Solution (Thermo Fisher Scientific) was added. Absorbance at 450 nm was measured using the Tecan Spark plate reader. Background absorbance was subtracted, and the data was analyzed by four-parameter nonlinear regression with GraphPad Prism software (v 9.2.0). The EC_{50} value was interpolated from the fitted curve.

Mouse Dose−Response Study. A mouse study was conducted by the Biological Resource Centre, Agency for Science, Technology and Research, Singapore, under a paid service agreement. Procedures were performed in accordance with approved IACUC protocol 211620. Female C57BL/6 were purchased from the InVivos Pte Ltd. and used at 6−8 weeks of age. Each group (n = 5) was administered ACM-S1S2(Beta) at 0.12, 0.6, 3, or 15 μg and ACM-CpG 1826 at 4, 20, or 100 μg per dose. Mice were anesthetized by isoflurane prior to injection. Material was given by IM injection (inner thigh muscle) at 100 μL per limb (200 μL total) in a 1 mL tuberculin syringe with a 30 G needle for two doses separated by 21 days. Blood was collected 20 days after prime and 14 days after boost to assess serum antibody titers; the spleen was collected 14 days after boost to assess T cell activity. In-life blood collection was performed by manually restraining the mouse followed by puncturing of the facial vein using a lancet of an appropriate size. 150−200 μL of blood was collected in a 1.5 mL snap-cap tube. Terminal bleed was done via a

https://doi.org/10.1021/acsnano.2c06350
ACS Nano 2022, 16, 16757−16775

cardiac puncture. The mouse was placed under full general anesthesia and laid in dorsal recumbency. Cardiac bleed was performed with a 23−25 G needle and 1 mL tuberculin syringe. Blood was allowed to clot for 30 min at room temperature and then centrifuged at 5500 rpm for a total of 10 min. Serum was collected and stored at −20 °C until analysis.

Mouse Serum IgG ELISA. In-house-purified recombinant spike protein (WT or Beta) was coated onto a high binding 96-well EIA/RIA plate (Corning) at 2 μg/mL in PBS (pH 7.4) overnight at 4 °C. The next morning, the plates were washed thrice with PBS + 0.1% v/v Tween-20 and blocked with 2% w/v BSA in wash buffer for 1.5 h at 37 °C. Mouse sera were serially diluted from an initial of ratio of 1:100 with blocking buffer, and the sample was applied to the plate for 1 h at 37 °C. HRP-conjugated goat antimouse IgG (H/L) (BioRad), antimouse IgG1 (BioRad), or antimouse IgG2c (BioRad) was diluted in blocking buffer at 1:10 000, 1:4000, and 1:4000, respectively (based on the manufacturer's recommendation), and applied to the plate for 1 h at 37 °C. Antibody binding was visualized by the addition of TMB substrate (Sigma-Aldrich) for 10 min at room temperature, and the reaction was terminated with Stop Solution (Thermo Fisher Scientific). Absorbance at 450 nm was measured using the Tecan Spark plate reader. Data was analyzed by five-parameter nonlinear regression with GraphPad Prism software (v 9.2.0). The end point titer, defined as the reciprocal of the highest dilution producing an absorbance three times the plate background, was interpolated from each titration curve.

Serum IgG titers against the ACM vector were assessed on the basis of a previously described method.[62] Briefly, ACM polymersomes were coated onto high binding 96-well EIA/RIA plates (Corning) at 50 μg/mL in PBS (pH 7.4) overnight at 4 °C. The next morning, plates were washed 4× with PBS and blocked with 5% w/v nonfat milk (Thermo Fisher Scientific) in PBS for 2 h at room temperature. Tween-20 was excluded from all buffers as it was reported to reduce assay sensitivity given its resemblance to polyethylene glycol (PEG).[63] Mouse sera were serially diluted from an initial ratio of 1:40 with 1% w/v nonfat milk and applied to the plate for 2 h at room temperature. After washing 4×, HRP-conjugated goat antimouse IgG (H/L) was diluted 1:10 000 in 1% w/v nonfat milk and applied to the plate for 1 h at room temperature. Visualization of antibody binding, data collection, and processing were subsequently performed, as described above.

***Ex Vivo* T Cell Stimulation Assay.** All reagents were purchased from Thermo Fisher Scientific unless stated otherwise. Splenocytes were mechanically dissociated by meshing through a 70 μm cell strainer. Red blood cells were lysed using RBC Lysis Buffer for 5 min at room temperature. The remaining cells were washed with FACS buffer (1× PBS + 2% v/v heat-inactivated fetal bovine serum + 1 mM EDTA) and transferred to a 96-well U-bottom plate at 2 million cells per well. Cells were treated with costimulatory CD28 (1 μg/mL), CD49d (1 μg/mL), and an overlapping peptide pool covering the spike S1 and S2 domains (1 μg/mL of each peptide; JPT Peptide Technologies) in complete T cell medium (RPMI supplemented with 10% heat-inactivated fetal bovine serum, 50 μM β-mercaptoethanol, 2 mM L-glutamax, 10 mM HEPES, and 100 U/mL penicillin/streptomycin). Nonpeptide-stimulated wells were treated with CD28 and CD49d. Splenocytes were incubated overnight at 37 °C and 5% CO_2. The following morning, 1× brefeldin A and 1× monensin (BioLegend) were added to each well to block the release of cytokines for 6 h.

Flow Cytometry. All antibodies and reagents were purchased from BioLegend, unless stated otherwise. Splenocytes were first stained with Fixable Viability Dye eFluor 455UV (Thermo Fisher Scientific) at a 1:1000 dilution in PBS for 30 min at 4 °C. Cells were washed with FACS Buffer and then incubated for 30 min at 4 °C with the following antibody clones to label the surface markers: BUV395-CD45 (30-F11; BD), BV785-CD3 (17A2), AF700-CD4 (GK1.5), APC-eFluor 780-CD8 (53−6.7; Thermo Fisher Scientific), and PE-Dazzle 594-CD44 (IM7). After washing, splenocytes were fixed and permeabilized using the Cytofix/Cytoperm buffer set (BD) according to manufacturer's instructions. Finally, cells were incubated for 30 min at 4 °C with the following antibody clones to label intracellular cytokines: AF488-IFNγ (XMG1.2), BV650-TNFα (MP6-XT22), APC-IL-2 (JES6-5H40), PerCP-eFluor 710-IL-4 (11B11; Thermo Fisher Scientific), and PE-IL-5 (TRFK5). After a final wash with 1× Permeabilization Buffer, cells were acquired using a LSRII flow cytometer. Approximately 1 million total events were captured for each sample. Data analysis was performed using FlowJo v10 (BD).

Hamster Immunogenicity Study. Hamster procedures, sample collection, and analyses were performed by Bioqual, Inc. (USA) under a paid service agreement. Procedures were performed in accordance with approved IACUC protocol 21-096P. Golden Syrian hamsters comprising equal numbers of males and females were purchased from Envigo, Charles River, and used at 6−8 weeks of age. Animals were immunized in an ABSL-2/BSL-2 facility. Each group (n = 8) was administered a placebo or a specific vaccine formulation via IM or IN administration. Each vaccine dose was standardized at 20 μg of spike protein and 100 μg of CpG for a total of two doses, 21 days apart. IM administration was performed in the thigh muscles at 100 μL per limb (200 μL total). The animal was restrained, and the injection site was cleaned with an alcohol swab before material was administered with an insulin needle and syringe (12.7 mm, 1/2 in.; BD). IN administration required the animal to be anesthetized with 80 mg/kg ketamine and 5 mg/kg xylazine via the IM route. Animals were then positioned upright, and material was administered at 50 μL per nostril, dropwise, using a P200 pipettor (100 μL total). Animals were then injected with antisedan at 1 mg/kg via the IM route approximately 30 min post-procedure and monitored until complete recovery. Blood and nasal wash were collected 20 days after the first dose and 13 days after the second dose. Blood was collected in 0.6 mL SST tubes (BD) from the retro-orbital vein under sedation and allowed to clot for 30 min to 1 h at room temperature. The samples were centrifuged at 1000−1300g for 5−10 min with the brakes off. Serum was collected and stored at −20 °C until analysis. A nasal wash was performed by first anesthetizing the animal with isoflurane and then placing it in lateral recumbency, followed by flushing 400 μL of PBS into the nasal cavity with a soft tipped catheter. A collection device was placed under the opposite nostril to collect the fluid. The nasal wash was stored at −20 °C until analysis.

Hamster Challenge Study. Fourteen days after the final vaccination, hamsters were transferred to an ABSL-3/BSL-3 facility and challenged with SARS-CoV-2 Beta variant [(2019-nCoV/South Africa/KRISP-K005325/2020)-p4 strain] at a dose of 3.67×10^2 PFU in 100 μL via IN inoculation (described above). Over the next 14 days, the hamsters were monitored for body weight changes and other clinical symptoms (mild ruffled fur; hunched; ruffled fur; lethargy/listlessness; weight loss >20%) and assigned a COVID score corresponding to severity (0 = normal; ≤2 = mild disease; 3 = moderate disease; ≥4 = severe disease). Oral swabs were performed on Days 2, 4, 7, and 14 post-challenge for viral RNA qPCR. Hamsters were restrained for sample collection. A sterile swab was removed from the packaging, and the oral cavity was swabbed once. The swab was placed into a cryovial with 1 mL of PBS; the shaft was cut off to fit into the vial, and the vial was placed immediately on dry ice for snap-freezing. The sample was then stored at −80 °C until analysis.

Histopathological Examination of the Lung. At necropsy, the left lung was collected and placed in 10% neutral buffered formalin. Tissue sections were trimmed and processed to hematoxylin and eosin (H&E) stained slides and examined by a board-certified pathologist at Experimental Pathology Laboratories, Inc. (EPL) in Sterling, Virginia. Histopathologic findings were graded from one to five, depending upon severity (1 = minimal; 2 = mild; 3 = moderate; 4 = marked; 5 = severe).

Hamster Serum IgG ELISA. Nunc MaxiSorp 96-well plates were coated with commercial recombinant spike (WT or Beta variant; Sino Biological) at 2 μg/mL in PBS (pH 7.4). Plates were incubated for 12 h at 37 °C. Unbound antigen was removed by washing three times with PBS + 0.05% v/v Tween-20. Plates were blocked in PBS + 5% w/v skim milk for 1 h at 37 °C. Test and positive control samples were diluted in assay diluent (1% w/v skim milk in wash buffer) to an initial dilution of 1:20 followed by a 4-fold serial dilution and applied

https://doi.org/10.1021/acsnano.2c06350
ACS Nano 2022, 16, 16757−16775

to the ELISA plate for 2 h at 37 °C. The plate was then washed thrice, and secondary detection antibody (goat antispecies-HRP IgG; Abcam) was added at a dilution of 1:10 000. Plates were incubated for 30 min at room temperature and then washed thrice. Bound antibodies were visualized by the addition of 1-Step Ultra TMB substrate (Thermo Fisher Scientific) for 10 min, and the reaction terminated with a TMB stop solution (SERA CARE). Absorbance at 450 nm was measured with the Thermo Labsystems Multiskan spectrophotometer. Data was analyzed by five-parameter nonlinear regression with GraphPad Prism software (v 9.2.0). Antibody titer, defined as the reciprocal of the highest dilution that gave a predefined cutoff value, was interpolated from the fitted curve.

SARS-CoV-2 Surrogate Virus Neutralization Test (cPass). The cPass kit (GenScript) was used according to the manufacturer's instructions. Briefly, each sample was diluted to a ratio of 1:10 using Sample Dilution Buffer and incubated with an equal volume of HRP-RBD (WT or variant) reagent for 30 min at 37 °C. The Omicron RBD sequence was based on the most prevalent mutations and reflect the dominant Omicron strain.[5] The mixture of serum and HRP-RBD was then applied to eight-well strips precoated with ACE2 protein for 15 min at 37 °C. Unbound RBD was washed off, and RBD-ACE2 binding was visualized by the addition of TMB substrate for 15 min at room temperature. The reaction was terminated using Stop Solution, and absorbance was measured at 450 nm. Inhibition of RBD-ACE2 binding was calculated using the formula: $\left(1 - \frac{\text{OD value of sample}}{\text{OD value of negative control}}\right) \times 100\%$. Where necessary, samples were pooled and concentrated using Vivaspin 500 centrifugal concentrators (MWCO 50 kDa; Sartorius) according to the manufacturer's instructions.

Plaque Reduction Neutralization Test (PRNT). Vero 76 cells were cultured in 24-well plates at 175 000 cells/well in DMEM + 10% v/v FBS + gentamicin and incubated at 37 °C and 5% CO_2. Cells were used at 90−100% confluency. Serum samples were heat inactivated at 56 °C for 30 min. A 30 PFU/well concentration of virus [USA-WA1/2020 strain or (2019-nCoV/South Africa/KRISP-K005325/2020)-p4 strain] was prepared and kept on ice until use. Each serum sample was first diluted 1:10 with DMEM + 2% v/v FBS + gentamicin, followed by 3-fold serial dilutions. An equal volume of 30 PFU/well virus inoculum was added to each serum dilution. Virus-only positive control and no-virus negative control were prepared in parallel. The mixes were incubated at 37 °C and 5% CO_2 for 1 h. Subsequently, Vero cell culture medium was removed from the 24-well plate, and 250 μL of titrated serum samples was added in duplicates. The 24-well plate was incubated at 37 °C and 5% CO_2 for 1 h for virus infection. During this time, 0.5% w/v methylcellulose medium was prewarmed in a 37 °C water bath. Subsequently, 1 mL of methylcellulose medium was added to each well, and the plate was incubated at 37 °C and 5% CO_2 for 3 days. The overlay medium was then removed, and Vero monolayers were washed once with 1 mL of PBS. Cells were fixed with 400 μL of ice-cold methanol per well at −20 °C for 30 min. After fixation, methanol was discarded and the monolayers were incubated with 400 μL per well of staining solution (0.2% w/v crystal violet, 20% v/v methanol, 80% v/v dH_2O) for 30 min at room temp. Wells were washed once with PBS or dH_2O and allowed to dry for ∼15 min. The plaques in each well were recorded, and the number of infectious units calculated.

Viral RNA Load Determination by qPCR. The amount of RNA copies per mL of oral swab was determined using a validated qRT-PCR assay. Viral RNA was first isolated from samples using a Qiagen DSP Virus/Pathogen Midi Kit and IVD Complex800 or IVD Cellfree500 protocols. The qRT-PCR assay utilized primers and a probe specifically designed to amplify and bind a conserved region of Envelop (E) gene of SARS-CoV-2 for the genomic RNA and Nucleocapsid (N) gene for subgenomic RNA detection. The signal was compared to a known standard curve and calculated to give copies per mL. To generate a control for the amplification reaction, RNA was isolated from the applicable SARS-CoV-2 plasmid control using the same procedure. qPCR was set up using a TaqMan Fast Virus 1-Step Real-time RT-PCR protocol with the assay setup performed using a Qiagen Qiagility automated PCR setup platform and analyzed in Applied Biosystems on QuantStudio 3.

Toxicological Study. A toxicological evaluation of the ACM-Beta spike vaccine was performed by the Department of Safety Assessment, Eurofins Advinus Limited, India, in compliance with GLP standards. This study plan has been approved by the Institutional Animal Ethics Committee (IAEC) of test facility Eurofins Advinus Limited (Proposal No.: 012/Aug-2020 dated 17 August 2020). New Zealand white rabbits were purchased from Liveon Biolabs Pvt. Ltd. and used at 4−5 months of age. Animals were randomized into a main study group comprising five males and five females and monitored for 30 days or a recovery group comprising two males and two females and monitored for 57 days. Dosing was performed on Days 0, 14, and 28 via the IM or IN route with 0.5 mL of placebo or ACM-S1S2(Beta) + ACM-CpG vaccine at 20 μg + 100 μg, respectively. IM injection was performed with a 261/2 in. G sterile needle at the quadriceps muscle. Injections 1 and 3 were administered to the left quadriceps muscle, and injection 2 was administered to the right quadriceps muscle. IN administration was performed using MAD. A volume of 0.25 mL was applied to each nostril for a total dose of 0.5 mL.

Clinical Signs and Mortality. Each animal was observed twice daily for mortality and morbidity. Routine observations for checking general clinical signs were performed at least twice (predose and postdose) on all the immunization days and daily once thereafter. A detailed clinical examination was performed 1 day prior to the initiation of treatment and once weekly thereafter during the in-life phase of the experiment. Animals were observed for changes in skin and fur, the injection site compared to the surrounding tissues, eyes, mucous membranes, autonomic activity, gait, and posture, the occurrence of secretions and excretions, and the response to handling as well as the presence of clonic or tonic movements, stereotypies, and bizarre behavior.

Local Reactions at the Site of Administration. IM and IN sites were evaluated for erythema and edema (none; very slight; well-defined; moderate to severe; severe) prior to each dose at approximately 2, 4, 6, and 8 h post-dose on all the cycles of immunization. The local reactions were assessed as per the numerical scoring system of Draize et al.[64]

Body Weights. Individual animal body weights were recorded at pretreatment (Day 0) and daily during the first week of administration and biweekly thereafter during treatment and recovery periods. The fasting body weight was recorded before necropsy.

Clinical Pathology. Clinical laboratory investigations were performed during the acclimatization period (pretreatment), on Day 2 (after the first dose) for the main group of rabbits, and at termination of the main and recovery groups (i.e., on Days 30 and 57, respectively). Blood was collected from the overnight fasted (water allowed) rabbits from the central (medial) ear artery. Approximately 0.7 mL of blood was collected in a K_2 EDTA tube for hematology; additionally, 1.8 mL of blood was collected in lithium heparin for clinical chemistry and 0.5 mL, in trisodium citrate for coagulation. Hematology was performed using the ADVIA 2120i Hematology System (Siemens Healthcare Diagnostics Inc.). Blood samples for coagulation analysis were centrifuged at 2500*g* and 15 °C for 10 min to separate the plasma and analyzed for the following parameters in the plasma sample using a STart Max Coagulation Analyzer (Diagnostica Stago Inc.). Plasma for clinical chemistry was analyzed using a Dimension RxL MaX Clinical Chemistry System (Dade Behring Inc.). Hematological parameters are described in Table S1; coagulation parameters are described in Table S2, and clinical chemistry parameters are described in Table S3.

C-Reactive Protein ELISA. Serum CRP was analyzed using the C Reactive Protein (PTX1) Rabbit ELISA Kit (Abacm) according to the manufacturer's instructions. Standards, the control, and samples were analyzed in duplicate. Duplicate readings were averaged, and the control blank reading was subtracted from all sample and standard readings. A standard curve was constructed using GraphPad Prism software. CRP concentrations of the samples were interpolated from the standard curve.

https://doi.org/10.1021/acsnano.2c06350
ACS Nano 2022, 16, 16757−16775

Urinalysis. Urine was collected from all the animals at pretreatment and at the termination of the main and recovery groups, prior to sacrifice. Collection was done from the Noryl litter tray placed below each cage and from the urinary bladder at termination. See Table S5 for the urinalysis parameters. Refractometry was performed using a PAL-10S Digital Hand-held Pocket Urine Specific Gravity Refractometer (ATAGO Co., Ltd.). Other parameters were measured using Multistix 10 SG strips and read with a Clinitek Advantus Analyzer (Siemens Healthcare diagnostics) or manually recorded.

Pathology. Necropsy was performed at the termination of the main and recovery groups. The rabbits fasted overnight (with an *ad libitum* supply of drinking water) prior to the scheduled necropsy. Rabbits to be sacrificed were weighed, deeply anaesthetized with intravenous administration of thiopentone sodium, exsanguinated, and subjected to a detailed necropsy by a veterinary pathologist.

Tissue Collection, Weighing, and Preservation. On completion of the gross pathology examination, tissues and organs noted below were collected and weighed from all rabbits. The paired organs were weighed together, and the combined weights were presented. The organ weight ratios (organ to body weight and organ to brain weight) were determined and presented in the report. The tissues were preserved in 10% neutral buffered formalin (NBF) except for the testes and eyes. See Table S6 for a list of organs examined.

Histopathology. A histopathological examination was carried out on the preserved organs of all the main and recovery group animals. In addition, injection sites and gross lesions were examined in all groups. The tissues were processed for routine paraffin embedding, and 5 μm sections were stained with Haematoxylin and Eosin stain. Unused tissues were archived. The individual animal microscopic findings along with the pathology narrative were shared with the peer review pathologist, and the tissue slides for the animal numbers indicated by the peer reviewer were shipped to the reviewer's address. The peer reviewed findings were documented and discussed, and the consensus diagnoses were presented in the pathology report. Microscopic findings (i.e., increased cellularity, hemorrhage, inflammatory infiltrate, and cell debris) were scored according to severity (minimal; mild; moderate; marked) or otherwise described as unremarkable.

Statistics. Analyses were done using GraphPad Prism software (v 9.2.0). Where appropriate, a one-way ANOVA with Tukey's multiple comparisons, a Brown-Forsythe and Welch ANOVA with Dunnett's T3 multiple comparisons, a two-way repeated measures ANOVA with Tukey's or Šidák's multiple comparisons, a two-tailed paired *t* test, or an unpaired *t* test with Welch's correction was performed. Significant differences were indicated where present, *: $P \leq 0.05$; **: $P \leq 0.01$; ***: $P \leq 0.001$; ****: $P \leq 0.0001$; ns: not significant. Data from the GLP toxicological study was captured with the Provantis integrated preclinical software (Instem), and the analysis was performed using the built-in statistical function.

ASSOCIATED CONTENT

Supporting Information

The Supporting Information is available free of charge at https://pubs.acs.org/doi/10.1021/acsnano.2c06350.

Expression and purification of S1S2 protein followed by its encapsulation within ACM polymersomes, dose−response study of ACM-S1S2(Beta) + ACM-CpG in C57BL/6 mice after IM administration, variation in body weights of male and female hamsters after a live SARS-CoV-2 Beta variant challenge, representative H&E images of hamster lungs after the Beta challenge, representative H&E images of a rabbit quadriceps muscle and nasal cavity at the conclusion of GLP toxicological study, table of hematological parameters, table of coagulation parameters, table of clinical chemistry parameters, table of altered hematological parameters of male rabbits after vaccination, table of urinalysis parameters, and table of organs subjected to anatomical and histopathological examination (PDF)

AUTHOR INFORMATION

Corresponding Authors

Madhavan Nallani − *ACM Biolabs Pte Ltd., 638075, Singapore*; Phone: +65 62655646; Email: mnallani@acmbiolabs.com

Pierre Vandepapeliere − *ACM Biosciences AG, 4051 Basel, Switzerland*; Email: pvandepapeliere@acmbiosciences.com

Authors

Jian Hang Lam − *ACM Biolabs Pte Ltd., 638075, Singapore*; orcid.org/0000-0003-3378-350X

Devendra Shivhare − *ACM Biolabs Pte Ltd., 638075, Singapore*

Teck Wan Chia − *ACM Biolabs Pte Ltd., 638075, Singapore*

Suet Li Chew − *ACM Biolabs Pte Ltd., 638075, Singapore*

Gaurav Sinsinbar − *ACM Biolabs Pte Ltd., 638075, Singapore*

Ting Yan Aw − *ACM Biolabs Pte Ltd., 638075, Singapore*

Siamy Wong − *ACM Biolabs Pte Ltd., 638075, Singapore*

Shrinivas Venkataraman − *ACM Biolabs Pte Ltd., 638075, Singapore*

Francesca Wei Inng Lim − *Department of Hematology, Singapore General Hospital, 169608, Singapore*

Complete contact information is available at: https://pubs.acs.org/10.1021/acsnano.2c06350

Author Contributions

M.N., J.H.L., S.V., F.W.L.L., and P.V. conceptualized and designed the experiments. D.S., T.W.C., S.L.C., S.V., G.S., T.Y.A., S.W., and J.H.L. performed the experiments. M.N. and F.W.I.L. acquired project funding. J.H.L., D.S., T.W.C., S.V., and M.N. analyzed the data. J.H.L., D.S., T.W.C., and M.N. wrote the manuscript. All authors have given approval to the final version of the manuscript.

Funding

This project has been funded by the NHIC Gap Funding Award (NHIC-COV19-2005008).

Notes

A preprint version of this work is available online: Jian Hang Lam; Devendra Shivhare; Teck Wan Chia; Suet Li Chew; Gaurav Sinsinbar; Ting Yan Aw; Siamy Wong; Shrinivas Venkataraman; Francesca Wei Inng Lim; Pierre Vandepapeliere; Madhavan Nallani. Next-generation intranasal Covid-19 vaccine: a polymersome-based protein subunit formulation that provides robust protection against multiple variants of concern and early reduction in viral load of the upper airway in the golden Syrian hamster model. *bioRxiv*; 10.1101/2022.02.12.480188 (accessed 2022-06-07).

The authors declare the following competing financial interest(s): J.H.L., D.S., T.W.C., S.L.C., S.V., G.S., T.Y.A., and S.W. are employees of ACM Biolabs Pte Ltd., Singapore. M.N. is the Chief Executive Officer of ACM Biolabs Pte Ltd., Singapore. P.V. is the acting Chief Medical Officer of ACM Biosciences AG, Basel, Switzerland.

ACKNOWLEDGMENTS

We would like to thank Ms. Joey Poh Soh Yee and the staff of BRC, A*STAR, Singapore, for performing mouse immuniza-

tion and sample collection; Dr. Swagata Kar and her team at Bioqual, Inc., U.S.A. for performing hamster experiments and sample analyses; Mr. S. B. Mohankumar and his team at the Department of Safety Assessment, Eurofins Advinus Limited, for conducting the toxicological investigation in rabbits. We would also like to thank Dr. Dennis Klinman and Ms. Katherine Schultheis for their critical reading, invaluable feedback, and editing of the manuscript.

REFERENCES

(1) Buchan, S. A.; Tibebu, S.; Daneman, N.; Whelan, M.; Vanniyasingam, T.; Murti, M.; Brown, K. A. Increased household secondary attacks rates with Variant of Concern SARS-CoV-2 index cases. *Clin Infect Dis* **2022**, *74*, 703−706.

(2) Dhar, M. S.; Marwal, R.; Vs, R.; Ponnusamy, K.; Jolly, B.; Bhoyar, R. C.; Sardana, V.; Naushin, S.; Rophina, M.; Mellan, T. A.; et al. Genomic characterization and epidemiology of an emerging SARS-CoV-2 variant in Delhi, India. *Science* **2021**, *374* (6570), 995−999.

(3) Fisman, D. N.; Tuite, A. R. Evaluation of the relative virulence of novel SARS-CoV-2 variants: a retrospective cohort study in Ontario, Canada. *Cmaj* **2021**, *193* (42), E1619−e1625.

(4) Planas, D.; Veyer, D.; Baidaliuk, A.; Staropoli, I.; Guivel-Benhassine, F.; Rajah, M. M.; Planchais, C.; Porrot, F.; Robillard, N.; Puech, J.; et al. Reduced sensitivity of SARS-CoV-2 variant Delta to antibody neutralization. *Nature* **2021**, *596* (7871), 276−280.

(5) Garcia-Beltran, W. F.; St Denis, K. J.; Hoelzemer, A.; Lam, E. C.; Nitido, A. D.; Sheehan, M. L.; Berrios, C.; Ofoman, O.; Chang, C. C.; Hauser, B. M.; et al. mRNA-based COVID-19 vaccine boosters induce neutralizing immunity against SARS-CoV-2 Omicron variant. *Cell* **2022**, *185*, 457.

(6) Liu, C.; Ginn, H. M.; Dejnirattisai, W.; Supasa, P.; Wang, B.; Tuekprakhon, A.; Nutalai, R.; Zhou, D.; Mentzer, A. J.; Zhao, Y.; et al. Reduced neutralization of SARS-CoV-2 B.1.617 by vaccine and convalescent serum. *Cell* **2021**, *184* (16), 4220−4236.e13.

(7) Greaney, A. J.; Loes, A. N.; Crawford, K. H. D.; Starr, T. N.; Malone, K. D.; Chu, H. Y.; Bloom, J. D. Comprehensive mapping of mutations in the SARS-CoV-2 receptor-binding domain that affect recognition by polyclonal human plasma antibodies. *Cell Host Microbe* **2021**, *29* (3), 463−476.e6.

(8) Planas, D.; Saunders, N.; Maes, P.; Guivel-Benhassine, F.; Planchais, C.; Buchrieser, J.; Bolland, W. H.; Porrot, F.; Staropoli, I.; Lemoine, F.; et al. Considerable escape of SARS-CoV-2 Omicron to antibody neutralization. *Nature* **2022**, *602*, 671.

(9) Cohn, B. A.; Cirillo, P. M.; Murphy, C. C.; Krigbaum, N. Y.; Wallace, A. W. SARS-CoV-2 vaccine protection and deaths among US veterans during 2021. *Science* **2022**, *375*, 331.

(10) Lopez Bernal, J.; Andrews, N.; Gower, C.; Gallagher, E.; Simmons, R.; Thelwall, S.; Stowe, J.; Tessier, E.; Groves, N.; Dabrera, G.; et al. Effectiveness of Covid-19 Vaccines against the B.1.617.2 (Delta) Variant. *N Engl J. Med.* **2021**, *385* (7), 585−594.

(11) Hu, Z.; Tao, B.; Li, Z.; Song, Y.; Yi, C.; Li, J.; Zhu, M.; Yi, Y.; Huang, P.; Wang, J. Effectiveness of inactivated COVID-19 vaccines against severe illness in B.1.617.2 (Delta) variant-infected patients in Jiangsu, China. *Int. J. Infect Dis* **2022**, *116*, 204−209.

(12) GeurtsvanKessel, C. H.; Geers, D.; Schmitz, K. S.; Mykytyn, A. Z.; Lamers, M. M.; Bogers, S.; Scherbeijn, S.; Gommers, L.; Sablerolles, R. S. G.; Nieuwkoop, N. N.; et al. Divergent SARS CoV-2 Omicron-reactive T- and B cell responses in COVID-19 vaccine recipients. *Sci. Immunol* **2022**, *7*, eabo2202.

(13) Keeton, R.; Tincho, M. B.; Ngomti, A.; Baguma, R.; Benede, N.; Suzuki, A.; Khan, K.; Cele, S.; Bernstein, M.; Karim, F.; et al. SARS-CoV-2 Spike T Cell Responses Induced Upon Vaccination or Infection Remain Robust against Omicron. *medRxiv* **2021** DOI: 10.1101/2021.12.26.21268380; https://www.medrxiv.org/content/10.1101/2021.12.26.21268380v1 (accessed 2022-01-18).

(14) Tarke, A.; Sidney, J.; Methot, N.; Yu, E. D.; Zhang, Y.; Dan, J. M.; Goodwin, B.; Rubiro, P.; Sutherland, A.; Wang, E.; et al. Impact of SARS-CoV-2 variants on the total CD4(+) and CD8(+) T cell reactivity in infected or vaccinated individuals. *Cell Rep. Med.* **2021**, *2* (7), 100355.

(15) Hewins, B.; Rahman, M.; Bermejo-Martin, J. F.; Kelvin, A. A.; Richardson, C. D.; Rubino, S.; Kumar, A.; Ndishimye, P.; Toloue Ostadgavahi, A.; Mahmud-Al-Rafat, A. Alpha, Beta, Delta, Omicron, and SARS-CoV-2 Breakthrough Cases: Defining Immunological Mechanisms for Vaccine Waning and Vaccine-Variant Mismatch. *Frontiers in Virology* **2022**, *2*, 849936.

(16) Wall, E. C.; Wu, M.; Harvey, R.; Kelly, G.; Warchal, S.; Sawyer, C.; Daniels, R.; Hobson, P.; Hatipoglu, E.; Ngai, Y.; et al. Neutralising antibody activity against SARS-CoV-2 VOCs B.1.617.2 and B.1.351 by BNT162b2 vaccination. *Lancet* **2021**, *397* (10292), 2331−2333.

(17) Garcia-Beltran, W. F.; Lam, E. C.; St Denis, K.; Nitido, A. D.; Garcia, Z. H.; Hauser, B. M.; Feldman, J.; Pavlovic, M. N.; Gregory, D. J.; Poznansky, M. C.; et al. Multiple SARS-CoV-2 variants escape neutralization by vaccine-induced humoral immunity. *Cell* **2021**, *184* (9), 2523.

(18) Dejnirattisai, W.; Huo, J.; Zhou, D.; Zahradník, J.; Supasa, P.; Liu, C.; Duyvesteyn, H. M. E.; Ginn, H. M.; Mentzer, A. J.; Tuekprakhon, A.; et al. Omicron-B.1.1.529 Leads to Widespread Escape from Neutralizing Antibody Responses. *bioRxiv* **2021** DOI: 10.1101/2021.12.03.471045; https://www.biorxiv.org/content/10.1101/2021.12.03.471045v2 (accessed 2022-01-18).

(19) Cele, S.; Gazy, I.; Jackson, L.; Hwa, S. H.; Tegally, H.; Lustig, G.; Giandhari, J.; Pillay, S.; Wilkinson, E.; Naidoo, Y.; et al. Escape of SARS-CoV-2 501Y.V2 from neutralization by convalescent plasma. *Nature* **2021**, *593* (7857), 142−146.

(20) Moyo-Gwete, T.; Madzivhandila, M.; Makhado, Z.; Ayres, F.; Mhlanga, D.; Oosthuysen, B.; Lambson, B. E.; Kgagudi, P.; Tegally, H.; Iranzadeh, A.; et al. Cross-Reactive Neutralizing Antibody Responses Elicited by SARS-CoV-2 501Y.V2 (B.1.351). *N Engl J. Med.* **2021**, *384* (22), 2161−2163.

(21) Lam, J. H.; Khan, A. K.; Cornell, T. A.; Chia, T. W.; Dress, R. J.; Yeow, W. W. W.; Mohd-Ismail, N. K.; Venkataraman, S.; Ng, K. T.; Tan, Y. J.; et al. Polymersomes as Stable Nanocarriers for a Highly Immunogenic and Durable SARS-CoV-2 Spike Protein Subunit Vaccine. *ACS Nano* **2021**, *15* (10), 15754−15770.

(22) Mohsen, M. O.; Gomes, A. C.; Cabral-Miranda, G.; Krueger, C. C.; Leoratti, F. M.; Stein, J. V.; Bachmann, M. F. Delivering adjuvants and antigens in separate nanoparticles eliminates the need of physical linkage for effective vaccination. *J. Controlled Release* **2017**, *251*, 92−100.

(23) van Doremalen, N.; Purushotham, J. N.; Schulz, J. E.; Holbrook, M. G.; Bushmaker, T.; Carmody, A.; Port, J. R.; Yinda, C. K.; Okumura, A.; Saturday, G. Intranasal ChAdOx1 nCoV-19/AZD1222 vaccination reduces viral shedding after SARS-CoV-2 D614G challenge in preclinical models. *Sci. Transl Med.* **2021**, *13* (607), eabh0755.

(24) Hsieh, C. L.; Goldsmith, J. A.; Schaub, J. M.; DiVenere, A. M.; Kuo, H. C.; Javanmardi, K.; Le, K. C.; Wrapp, D.; Lee, A. G.; Liu, Y.; et al. Structure-based design of prefusion-stabilized SARS-CoV-2 spikes. *Science* **2020**, *369* (6510), 1501−1505.

(25) Riley, T. P.; Chou, H. T.; Hu, R.; Bzymek, K. P.; Correia, A. R.; Partin, A. C.; Li, D.; Gong, D.; Wang, Z.; Yu, X.; et al. Enhancing the Prefusion Conformational Stability of SARS-CoV-2 Spike Protein Through Structure-Guided Design. *Front Immunol* **2021**, *12*, 660198.

(26) Krieg, A. M.; Efler, S. M.; Wittpoth, M.; Al Adhami, M. J.; Davis, H. L. Induction of systemic TH1-like innate immunity in normal volunteers following subcutaneous but not intravenous administration of CPG 7909, a synthetic B-class CpG oligodeoxynucleotide TLR9 agonist. *J. Immunother* **2004**, *27* (6), 460−471.

(27) Scheiermann, J.; Klinman, D. M. Clinical evaluation of CpG oligonucleotides as adjuvants for vaccines targeting infectious diseases and cancer. *Vaccine* **2014**, *32* (48), 6377−6389.

(28) Brito, L. A.; Singh, M. Acceptable levels of endotoxin in vaccine formulations during preclinical research. *J. Pharm. Sci.* **2011**, *100* (1), 34−37.

(29) McCluskie, M. J.; Davis, H. L. CpG DNA is a potent enhancer of systemic and mucosal immune responses against hepatitis B surface antigen with intranasal administration to mice. *J. Immunol* **1998**, *161* (9), 4463−4466.
(30) Xie, H.; Gursel, I.; Ivins, B. E.; Singh, M.; O'Hagan, D. T.; Ulmer, J. B.; Klinman, D. M. CpG oligodeoxynucleotides adsorbed onto polylactide-co-glycolide microparticles improve the immunogenicity and protective activity of the licensed anthrax vaccine. *Infect. Immun.* **2005**, *73* (2), 828−833.
(31) von Hunolstein, C.; Mariotti, S.; Teloni, R.; Alfarone, G.; Romagnoli, G.; Orefici, G.; Nisini, R. The adjuvant effect of synthetic oligodeoxynucleotide containing CpG motif converts the anti-Haemophilus influenzae type b glycoconjugates into efficient anti-polysaccharide and anti-carrier polyvalent vaccines. *Vaccine* **2001**, *19* (23−24), 3058−3066.
(32) Eastcott, J. W.; Holmberg, C. J.; Dewhirst, F. E.; Esch, T. R.; Smith, D. J.; Taubman, M. A. Oligonucleotide containing CpG motifs enhances immune response to mucosally or systemically administered tetanus toxoid. *Vaccine* **2001**, *19* (13−14), 1636−1642.
(33) Nazeri, S.; Zakeri, S.; Mehrizi, A. A.; Sardari, S.; Djadid, N. D. Measuring of IgG2c isotype instead of IgG2a in immunized C57BL/6 mice with Plasmodium vivax TRAP as a subunit vaccine candidate in order to correct interpretation of Th1 versus Th2 immune response. *Exp Parasitol* **2020**, *216*, 107944.
(34) Mallory, R.; Formica, N.; Pfeiffer, S.; Wilkinson, B.; Marcheschi, A.; Albert, G.; McFall, H.; Robinson, M.; Plested, J. S.; Zhu, M.; et al. Immunogenicity and Safety following a Homologous Booster Dose of a SARS-CoV-2 Recombinant Spike Protein Vaccine (NVX-CoV2373): A Phase 2 Randomized Placebo-Controlled Trial. *medRxiv* **2021** DOI: 10.1101/2021.12.23.21267374; https://www.medrxiv.org/content/10.1101/2021.12.23.21267374v1 (accessed 2022-01-19).
(35) Tan, C. W.; Chia, W. N.; Qin, X.; Liu, P.; Chen, M. I.; Tiu, C.; Hu, Z.; Chen, V. C.; Young, B. E.; Sia, W. R.; et al. A SARS-CoV-2 surrogate virus neutralization test based on antibody-mediated blockage of ACE2-spike protein-protein interaction. *Nat. Biotechnol.* **2020**, *38* (9), 1073−1078.
(36) Greaney, A. J.; Starr, T. N.; Eguia, R. T.; Loes, A. N.; Khan, K.; Karim, F.; Cele, S.; Bowen, J. E.; Logue, J. K.; Corti, D.; et al. A SARS-CoV-2 Variant Elicits an Antibody Response with a Shifted Immunodominance Hierarchy. *bioRxiv* **2021** DOI: 10.1101/2021.10.12.4641; https://www.biorxiv.org/content/10.1101/2021.10.12.464114v1 (accessed 2022-01-19).
(37) Sheward, D. J.; Mandolesi, M.; Urgard, E.; Kim, C.; Hanke, L.; Perez Vidakovics, L.; Pankow, A.; Smith, N. L.; Castro Dopico, X.; McInerney, G. M.; et al. Beta RBD boost broadens antibody-mediated protection against SARS-CoV-2 variants in animal models. *Cell Rep. Med.* **2021**, *2* (11), 100450.
(38) Horiuchi, S.; Oishi, K.; Carrau, L.; Frere, J.; Møller, R.; Panis, M.; tenOever, B. R. Immune memory from SARS-CoV-2 infection in hamsters provides variant-independent protection but still allows virus transmission. *Sci. Immunol* **2021**, *6* (66), eabm3131.
(39) Yuan, L.; Zhu, H.; Wu, K.; Zhou, M.; Ma, J.; Chen, R.; Tang, Q.; Cheng, T.; Guan, Y.; Xia, N. Female sex hormone, progesterone, ameliorates the severity of SARS-CoV-2-caused pneumonia in the Syrian hamster model. *Signal Transduct Target Ther* **2022**, *7* (1), 47.
(40) Wölfel, R.; Corman, V. M.; Guggemos, W.; Seilmaier, M.; Zange, S.; Müller, M. A.; Niemeyer, D.; Jones, T. C.; Vollmar, P.; Rothe, C.; et al. Virological assessment of hospitalized patients with COVID-2019. *Nature* **2020**, *581* (7809), 465−469.
(41) Afkhami, S.; D'Agostino, M. R.; Zhang, A.; Stacey, H. D.; Marzok, A.; Kang, A.; Singh, R.; Bavananthasivam, J.; Ye, G.; Luo, X.; et al. Respiratory mucosal delivery of next-generation COVID-19 vaccine provides robust protection against both ancestral and variant strains of SARS-CoV-2. *Cell* **2022**, *185* (5), 896−915.e19.
(42) van der Ley, P. A.; Zariri, A.; van Riet, E.; Oosterhoff, D.; Kruiswijk, C. P. An Intranasal OMV-Based Vaccine Induces High Mucosal and Systemic Protecting Immunity Against a SARS-CoV-2 Infection. *Front Immunol* **2021**, *12*, 781280.
(43) Krammer, F. SARS-CoV-2 vaccines in development. *Nature* **2020**, *586* (7830), 516−527.
(44) See, R. H.; Zakhartchouk, A. N.; Petric, M.; Lawrence, D. J.; Mok, C. P. Y.; Hogan, R. J.; Rowe, T.; Zitzow, L. A.; Karunakaran, K. P.; Hitt, M. M.; et al. Comparative evaluation of two severe acute respiratory syndrome (SARS) vaccine candidates in mice challenged with SARS coronavirus. *J. Gen Virol* **2006**, *87* (Pt 3), 641−650.
(45) Morokutti, A.; Muster, T.; Ferko, B. Intranasal vaccination with a replication-deficient influenza virus induces heterosubtypic neutralising mucosal IgA antibodies in humans. *Vaccine* **2014**, *32* (17), 1897−1900.
(46) Xia, H.; Zou, J.; Kurhade, C.; Cai, H.; Yang, Q.; Cutler, M.; Cooper, D.; Muik, A.; Jansen, K. U.; Xie, X.; et al. Neutralization of Omicron SARS-CoV-2 by 2 or 3 Doses of BNT162b2 Vaccine. *bioRxiv* **2022** DOI: 10.1101/2022.01.21.476344; https://www.biorxiv.org/content/10.1101/2022.01.21.476344v1 (accessed 2022-01-23).
(47) Gagne, M.; Moliva, J. I.; Foulds, K. E.; Andrew, S. F.; Flynn, B. J.; Werner, A. P.; Wagner, D. A.; Teng, I.-T.; Lin, B. C.; Moore, C.; et al. mRNA-1273 or mRNA-Omicron Boost in Vaccinated Macaques Elicits Comparable B Cell Expansion, Neutralizing Antibodies and Protection against Omicron. *bioRxiv* **2022** DOI: 10.1101/2022.02.03.479037; https://www.biorxiv.org/content/10.1101/2022.02.03.479037v1 (accessed 2022-02-05).
(48) McMahan, K.; Giffin, V.; Tostanoski, L. H.; Chung, B.; Siamatu, M.; Suthar, M. S.; Halfmann, P.; Kawaoka, Y.; Piedra-Mora, C.; Martinot, A. J.; et al. Reduced Pathogenicity of the SARS-CoV-2 Omicron Variant in Hamsters. *bioRxiv* **2022** DOI: 10.1101/2022.01.02.474743; https://www.biorxiv.org/content/10.1101/2022.01.02.474743v1 (accessed 2022-02-05).
(49) Peacock, T. P.; Brown, J. C.; Zhou, J.; Thakur, N.; Sukhova, K.; Newman, J.; Kugathasan, R.; Yan, A. W. C.; Furnon, W.; De Lorenzo, G.; Cowton, V. M.; Reuss, D.; et al. The Altered Entry Pathway and Antigenic Distance of the SARS-CoV-2 Omicron Variant Map to Separate Domains of Spike Protein. *bioRxiv* **2022** DOI: 10.1101/2021.12.31.474653; https://www.biorxiv.org/content/10.1101/2021.12.31.474653v2 (accessed 2022-10-11).
(50) Al-Halifa, S.; Gauthier, L.; Arpin, D.; Bourgault, S.; Archambault, D. Nanoparticle-Based Vaccines Against Respiratory Viruses. *Front Immunol* **2019**, *10*, 22.
(51) Kiyono, H.; Fukuyama, S. NALT- versus Peyer's-patch-mediated mucosal immunity. *Nat. Rev. Immunol* **2004**, *4* (9), 699−710.
(52) Childers, N. K.; Tong, G.; Mitchell, S.; Kirk, K.; Russell, M. W.; Michalek, S. M. A controlled clinical study of the effect of nasal immunization with a Streptococcus mutans antigen alone or incorporated into liposomes on induction of immune responses. *Infect. Immun.* **1999**, *67* (2), 618−623.
(53) Thomas, C.; Rawat, A.; Hope-Weeks, L.; Ahsan, F. Aerosolized PLA and PLGA nanoparticles enhance humoral, mucosal and cytokine responses to hepatitis B vaccine. *Mol. Pharmaceutics* **2011**, *8* (2), 405−415.
(54) Slütter, B.; Bal, S.; Keijzer, C.; Mallants, R.; Hagenaars, N.; Que, I.; Kaijzel, E.; van Eden, W.; Augustijns, P.; Löwik, C.; et al. Nasal vaccination with N-trimethyl chitosan and PLGA based nanoparticles: nanoparticle characteristics determine quality and strength of the antibody response in mice against the encapsulated antigen. *Vaccine* **2010**, *28* (38), 6282−6291.
(55) Knight, F. C.; Gilchuk, P.; Kumar, A.; Becker, K. W.; Sevimli, S.; Jacobson, M. E.; Suryadevara, N.; Wang-Bishop, L.; Boyd, K. L.; Crowe, J. E., Jr; et al. Mucosal Immunization with a pH-Responsive Nanoparticle Vaccine Induces Protective CD8(+) Lung-Resident Memory T Cells. *ACS Nano* **2019**, *13* (10), 10939−10960.
(56) Sheets, R. L.; Stein, J.; Manetz, T. S.; Andrews, C.; Bailer, R.; Rathmann, J.; Gomez, P. L. Toxicological safety evaluation of DNA plasmid vaccines against HIV-1, Ebola, Severe Acute Respiratory Syndrome, or West Nile virus is similar despite differing plasmid backbones or gene-inserts. *Toxicol. Sci.* **2006**, *91* (2), 620−630.

(57) Pati, R.; Shevtsov, M.; Sonawane, A. Nanoparticle Vaccines Against Infectious Diseases. *Front Immunol* **2018**, *9*, 2224.
(58) Thorp, E. B.; Boada, C.; Jarbath, C.; Luo, X. Nanoparticle Platforms for Antigen-Specific Immune Tolerance. *Front Immunol* **2020**, *11*, 945.
(59) Sanità, G.; Carrese, B.; Lamberti, A. Nanoparticle Surface Functionalization: How to Improve Biocompatibility and Cellular Internalization. *Front Mol. Biosci* **2020**, *7*, 587012.
(60) Ndeupen, S.; Qin, Z.; Jacobsen, S.; Bouteau, A.; Estanbouli, H.; Igyártó, B. Z. The mRNA-LNP platform's lipid nanoparticle component used in preclinical vaccine studies is highly inflammatory. *iScience* **2021**, *24* (12), 103479.
(61) Janakiraman, V.; Forrest, W. F.; Seshagiri, S. Estimation of baculovirus titer based on viable cell size. *Nat. Protoc* **2006**, *1* (5), 2271−2276.
(62) Yang, Q.; Jacobs, T. M.; McCallen, J. D.; Moore, D. T.; Huckaby, J. T.; Edelstein, J. N.; Lai, S. K. Analysis of Pre-existing IgG and IgM Antibodies against Polyethylene Glycol (PEG) in the General Population. *Anal. Chem.* **2016**, *88* (23), 11804−11812.
(63) Sherman, M. R.; Williams, L. D.; Sobczyk, M. A.; Michaels, S. J.; Saifer, M. G. Role of the methoxy group in immune responses to mPEG-protein conjugates. *Bioconjug Chem.* **2012**, *23* (3), 485−499.
(64) Draize, J. H.; Woodard, G.; Calvery, H. O. Methods for the Study of Irritation and Toxicity of Substances Applied Topically to the Skin and Mucous Membranes. *J. Pharmacol. Exp. Ther.* **1944**, *82* (3), 377−390.

https://doi.org/10.1021/acsnano.2c06350
ACS Nano 2022, 16, 16757−16775